THE OHIO STATE UNIVERSITY

An Extended UTD Analysis for the Scattering and Diffraction from Cubic Polynomial Strips

E.D. Constantinides and R.J. Marhefka

The Ohio State University

ElectroScience Laboratory

Department of Electrical Engineering
Columbus, Ohio 43212

Final Report 725311-2
Grant No. NSG-1498
January 1993

National Aeronautics and Space Administration
Langley Research Center
Hampton, VA 23665

A. Approved for public release; Distribution is unlimited

NOTICES

When Government drawings, specifications, or other data are used for any purpose other than in connection with a definitely related Government procurement operation, the United States Government thereby incurs no responsibility nor any obligation whatsoever, and the fact that the Government may have formulated, furnished, or in any way supplied the said drawings, specifications, or other data, is not to be regarded by implication or otherwise as in any manner licensing the holder or any other person or corporation, or conveying any rights or permission to manufacture, use, or sell any patented invention that may in any way be related thereto.

50272-101

REPORT DOCUMENTATION PAGE	1. REPORT NO.	2.	3. Recipient's Accession No.

4. Title and Subtitle
An Extended UTD Analysis for the Scattering and Diffraction from Cubic Polynomial Strips

5. Report Date
January 1993

6.

7. Author(s)
E.D. Constantinides and R.J. Marhefka

8. Performing Org. Rept. No.
725311-2

9. Performing Organization Name and Address
The Ohio State University
ElectroScience Laboratory
1320 Kinnear Road
Columbus, OH 43212

10. Project/Task/Work Unit No.

11. Contract(C) or Grant(G) No.
(C)
(G) NSG-1498

12. Sponsoring Organization Name and Address
National Aeronautics and Space Administration
Langley Research Center
Hampton, VA 23665

13. Report Type/Period Covered
Final Report

14.

15. Supplementary Notes

16. Abstract (Limit: 200 words)

Spline and polynomial type surfaces are commonly used in high frequency modeling of complex structures such as aircraft, ships, reflectors, etc. It is therefore of interest to develop an efficient and accurate solution to describe the scattered fields from such surfaces. In this report an extended UTD solution for the scattering and diffraction from perfectly conducting cubic polynomial strips is derived and involves the incomplete Airy integrals as canonical functions. This new solution is universal in nature and can be used to effectively describe the scattered fields from flat, strictly concave or convex, and concave-convex boundaries containing edges. The classic UTD solution fails to describe the more complicated field behavior associated with higher order phase catastrophes and therefore a new set of uniform reflection and first-order edge diffraction coefficients is derived. Also, an additional diffraction coefficient associated with a zero-curvature (inflection) point is presented. Higher order effects such as double edge diffraction, creeping waves, and whispering gallery modes are not examined in this work. The extended UTD solution is independent of the scatterer size and also provides useful physical insight into the various scattering and diffraction processes. Its accuracy is confirmed via comparison with some reference moment method results.

17. Document Analysis a. Descriptors
ASYMPTOTIC
DIFFRACTION
SCATTERING
2-D
UTD (UNIFORM THEORY OF DIFFRACTION)

b. Identifiers/Open-Ended Terms

c. COSATI Field/Group

18. Availability Statement
A. Approved for public release;
Distribution is unlimited.

19. Security Class (This Report)
Unclassified

21. No. of Pages
53

20. Security Class (This Page)
Unclassified

22. Price

(See ANSI-Z39.18) *See Instructions on Reverse* OPTIONAL FORM 272 (4-77)
Department of Commerce

Contents

List of Figures

Chapter 1

Introduction

High frequency electromagnetic analysis of problems involving complex geometry descriptions of the scattering bodies has been of great interest in recent years. Spline and polynomial type surfaces are commonly used in high frequency modeling of complex structures such as aircraft, ships, reflectors, etc., and is therefore of interest to develop efficient and accurate solutions for the purpose of RCS and antenna pattern predictions. Numerical techniques for treating these problems such as Physical Optics (PO) [1] and the Method of Moments (MM) [2], while simple in concept, still require vast amount of computer resources for even intermediate sized targets. The use of closed form ray optical solutions, whenever possible, is one way to increase efficiency and also provide important physical insight into the various scattering and diffraction processes.

In many instances, high-frequency scattering and diffraction mechanisms can be described in terms of ray optical fields that behave locally like plane waves propagating along the trajectories of the Geometrical Optics (GO) [3] and the Geometrical Theory of Diffraction (GTD) [4]. Although these rather simple ray optical techniques can be used to solve many complex practical electromagnetic scattering/radiation problems, they fail to describe the more complicated field behavior inside transition regions where wave focusing due to higher order phase catastrophes and or changes from illuminated to shadow zones occur. Removing the errors within these regions

would greatly enhance the applicability of GTD as indeed has been shown for its uniform version, the so called UTD [5]. The UTD approach for dealing with transitional field behavior involves the use of appropriate transition functions that eliminate the errors of GO/GTD solutions, and also provide a smooth connection into the regions where these classical ray optical formulations remain valid.

A common method of analysis for high-frequency scattering and diffraction problems involves the use of radiation integrals as well as plane wave integral representations for the fields, with the asymptotic approximations for the various scattering mechanisms found from the critical point contributions of the integrand. This method of analysis when applied to a cubic polynomial surface containing an edge results in a stationary phase integral characterized by two stationary phase points that are arbitrarily close to one another or to an integration endpoint. Uniform asymptotic evaluation of integrals with such analytical properties involves the incomplete Airy function [6] which serves as a canonical integral for the description of transition region phenomena associated with composite shadow boundaries. Transition regions of such type result from the merging of the reflection shadow boundary associated with an edge in the scattering surface, and the smooth caustic of reflected rays arising from the confluence of the two stationary phase points near a zero-curvature (inflection) point. When the reflection shadow boundary is not in the immediate vicinity of the smooth caustic the conventional UTD diffraction coefficient [5] which involves the Fresnel integral as a canonical function can be used to effectively describe the edge diffracted fields. Furthermore, the ordinary Airy integrals and their derivatives are the appropriate canonical functions for the description of the high-frequency fields in the neighborhood of the smooth caustic [7]. However, when there is a confluence of both reflected and caustic type shadow boundaries, neither the Fresnel integral nor the ordinary Airy integrals adequately describe the transition region phenomena, and they must be appropriately replaced by the incomplete Airy functions. Although these functions are not so easily generated [8] as, for example,

the Fresnel integral or the complete Airy functions, a method for their efficient and accurate computation was recently developed [9] and allows for the formulation of uniform asymptotic solutions that are useful for engineering purposes.

In this report, an extended UTD solution for the scattering and diffraction from perfectly conducting cubic polynomial strips is derived and involves the incomplete Airy integrals as canonical functions. The scattering mechanisms involved are described by a new set of uniform reflection, first-order edge and zero-curvature diffraction coefficients that remain valid inside the transition regions and also provide smooth connection into the regions where the classic ray optical formulations still apply. Although additional higher order mechanisms such as creeping waves, double edge diffraction, and whispering gallery modes may also exist for the geometries considered, they will not be examined in this report. Also, this new solution is universal in nature and can be used to effectively describe the scattered fields from flat, strictly concave or convex, and concave-convex boundaries containing edges. Numerical results obtained using the extended UTD solution showed excellent agreement with the method of moments for both polarizations, except for some limited regions in the non-specular direction for the TE polarization where the higher order mechanisms become significant.

The outline of this report is as follows: In Chapter 2, a uniform asymptotic analysis for the plane wave scattering from a perfectly conducting cubic polynomial boundary containing an edge is presented, and in Chapter 3 the extended UTD solution for the scattering and diffraction from cubic polynomial strips is formulated. In Chapter 4, some indicative numerical results are presented and discussed with their accuracy confirmed via comparison with reference moment method results. In addition, results obtained using classic UTD are also shown to illustrate the need for the new solution. Finally, some concluding remarks and the accomplishments of this work are summarized in Chapter 5.

It is assumed that all fields are time harmonic with time dependence $e^{j\omega t}$, which will be suppressed throughout this report. Also, the medium surrounding the scatterers is assumed to be free space.

Chapter 2

Uniform Asymptotic Analysis

In this chapter, a uniform asymptotic analysis for predicting the scattered fields from perfectly conducting cubic polynomial strips is presented. The relevant canonical geometry for the analysis that follows is a semi-infinite two-dimensional cubic polynomial boundary illuminated by a plane wave as shown in Figure 2.1. The scattering mechanisms to be examined, namely specular reflection, zero-curvature and first-order edge diffraction are illustrated in Figure 2.2. As a plane parametric curve the boundary C is given by:

$$\vec{r}'(Q') = \hat{x}x + \hat{y}y(x) \; ; \quad a \leq x < \infty \tag{2.1}$$

where

$$y(x) = a_0 + a_1 x + a_2 x^2 + a_3 x^3 \, . \tag{2.2}$$

The zero-curvature point, x_p, is a root of the second derivative of the surface, i.e., $y''(x_p) = 0$ and is given by:

$$x_p \doteq \frac{-a_2}{3a_3} \, . \tag{2.3}$$

The scattered fields at any point P away from the surface boundary can be expressed in terms of the usual radiation integrals over the electric current $\vec{J}_s$ induced on the boundary by the incident plane wave as follows:

$$\vec{E}^s(P) \simeq \frac{kZ_0}{4} \int_C [\hat{s} \times \hat{s} \times \vec{J}_s(Q')] H_0^{(2)}(kr) \, dl' \;\; \text{(TM case)} \tag{2.4}$$

$$\vec{H}^s(P) \simeq \frac{k}{4} \int_C [\vec{J}_s(Q') \times \hat{s}] H_0^{(2)}(kr) \, dl' \;\; \text{(TE case)} \tag{2.5}$$

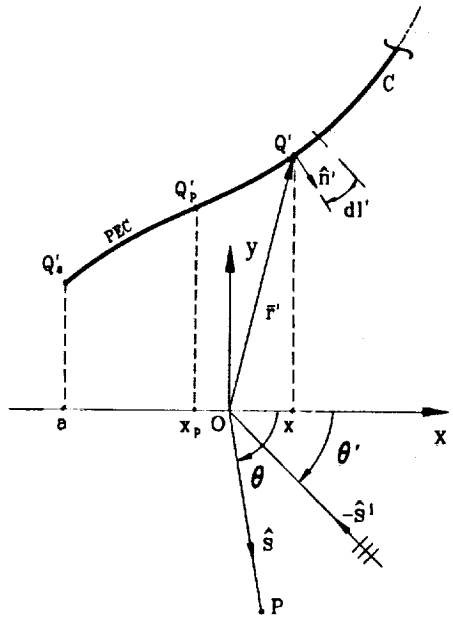

Figure 2.1: Canonical geometry for the uniform asymptotic analysis

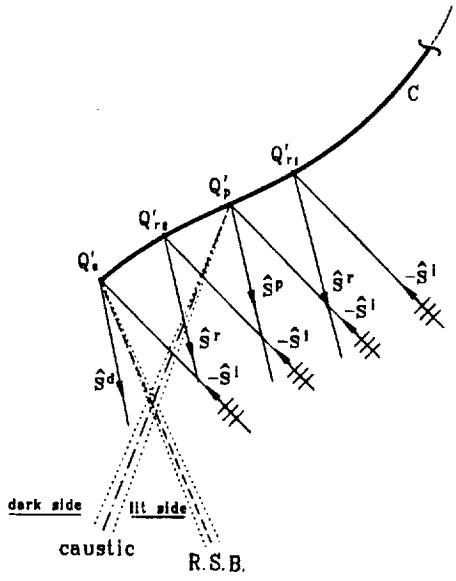

Figure 2.2: Scattering mechanisms associated with a cubic polynomial boundary containing an edge.

where

$$
\begin{aligned}
r &= |\overline{Q'P}| \simeq \rho - \vec{r}\,'(Q') \cdot \hat{s} \quad \text{(far-zone approximation)}, \\
\hat{s} &= \hat{x}\cos\theta + \hat{y}\sin\theta\,, \\
\vec{J}_s(Q') &= \text{value of } \vec{J}_s \text{ at any point } Q' \text{ on the surface}, \\
H_0^{(2)}(kr) &= \text{cylindrical Hankel function of the second kind of order zero}, \\
Z_0 &= \text{impedance of free space}, \\
k &= \text{wavenumber of free space, and} \\
dl' &= \text{line integration element.}
\end{aligned}
$$

In the PO approximation to (2.4) and (2.5), the induced current is assumed to be given by GO as follows:

$$
\vec{J}_s(Q') \approx \begin{cases} 2\hat{n}' \times \vec{H}^i(Q'), & \text{on the lit portion of the boundary} \\ 0\,, & \text{on the shadowed portion of the boundary} \end{cases} \tag{2.6}
$$

in which $\hat{n}'$ is the outward normal to the surface and $\vec{H}^i(Q')$ is the incident magnetic field at Q' that under the plane wave incidence assumption is given by:

$$
\vec{H}^i(Q') = \begin{cases} Z_0^{-1}(\hat{z} \times \hat{s}^i)e^{jk(\vec{r}\,'\cdot\hat{s}^i)} & \text{(TM case)} \\ \hat{z}e^{jk(\vec{r}\,'\cdot\hat{s}^i)} & \text{(TE case)} \end{cases} \tag{2.7}
$$

where

$$
\hat{s}^i = \hat{x}\cos\theta' + \hat{y}\sin\theta'\,. \tag{2.8}
$$

Using the assumed current in (2.6) and the large argument form of $H_0^{(2)}(kr)$ given by:

$$
H_0^{(2)}(kr) \sim \sqrt{\frac{2j}{\pi kr}}\, e^{-jkr}\,, \quad \text{for } kr \gg 1 \tag{2.9}
$$

the far-zone scattered field assumes the form:

$$
U_z^s(\rho;\theta',\theta) \simeq \mp\sqrt{\frac{jk}{2\pi}}\, e_{s,h}(\theta',\theta)\, \frac{e^{-jk\rho}}{\sqrt{\rho}} \tag{2.10}
$$

where $e_{s,h}(\theta',\theta)$ is the angular field dependence and is given by the stationary phase integral

$$e_{s,h}(\theta',\theta) = \int_a^\infty f_{s,h}(x) e^{jk\phi(x)}\, dx \tag{2.11}$$

where

$$f_{s,h}(x) = \frac{dl'}{dx}\hat{n}'(Q') \cdot \left\{ \begin{array}{c} \hat{s}^i \\ \hat{s} \end{array} \right\}, \tag{2.12}$$

$$\phi(x) = \vec{r}\,'(Q') \cdot (\hat{s}^i + \hat{s}) = xC(\theta',\theta) + y(x)S(\theta',\theta), \tag{2.13}$$

$$C(\theta',\theta) = \cos\theta' + \cos\theta, \tag{2.14}$$

$$S(\theta',\theta) = \sin\theta' + \sin\theta, \tag{2.15}$$

$$\frac{dl'}{dx} = h(x) = \sqrt{1 + [y'(x)]^2}, \text{ and} \tag{2.16}$$

$$\hat{n}'(Q') = \frac{\hat{x}y'(x) - \hat{y}}{h(x)}. \tag{2.17}$$

The next step in this procedure is the uniform asymptotic evaluation of $e_{s,h}(\theta',\theta)$ given in Equation (2.11).

2.1 Uniform Asymptotic Evaluation of $e_{s,h}(\theta',\theta)$

The integral in (2.11) can be transformed into a canonical form by first expanding the phase function in a Taylor series around the zero-curvature point x_p, i.e.,

$$\phi(x) = \phi(x_p) + (x - x_p)\phi'(x_p) + \frac{(x - x_p)^3}{3}\phi'''(x_p). \tag{2.18}$$

Notice that the above expansion is exact since $\phi''(x_p) = 0$ and $\phi^{(n)}(x) \equiv 0$ for every x with $n > 3$. Next we make the following linear transformation:

$$\phi(x) = \tau(s) = \alpha + \beta s + s^3/3, \tag{2.19}$$

where

$$\alpha = \tau(0) = \phi(x_p), \text{ and} \tag{2.20}$$

$$\beta = \phi'(x_p)\left[\frac{2}{\phi'''(x_p)}\right]^{\frac{1}{3}}. \tag{2.21}$$

The proper branch for β depends on the sign of $\phi'(x_p)$ and $\phi'''(x_p)$, thus

$$\beta = \begin{cases} \pm|\beta|e^{-j\frac{\pi}{3}} & \text{if } \phi'''(x_p) \leq 0 \\ \pm|\beta| & \text{if } \phi'''(x_p) > 0 \end{cases}, \quad \pm \text{ for } \phi'(x_p) \gtrless 0 \tag{2.22}$$

where

$$|\beta| = |\phi'(x_p)| \left| \frac{2}{\phi'''(x_p)} \right|^{\frac{1}{3}} . \tag{2.23}$$

Also, alternative expressions for α and β may be found directly from Equation (2.19), i.e.,

$$\alpha = \tau(s_{1,2}) + \frac{2}{3}(-\beta)^{\frac{3}{2}} \tag{2.24}$$

$$\beta = -\left\{ \frac{3}{2}[\tau(0) - \tau(s_{1,2})] \right\}^{\frac{2}{3}} \tag{2.25}$$

where $s_{1,2} = \pm(-\beta)^{1/2}$ are the stationary phase points satisfying $\tau'(s_{1,2}) = 0$. Thus, using Equation (2.19), the scattered field angular dependence, $e_{s,h}(\theta', \theta)$, becomes:

$$e_{s,h}(\theta', \theta) = \int_{\xi_a}^{\text{"}\infty\text{"}} G_{s,h}(s) e^{jk\tau(s)}\, ds \tag{2.26}$$

where

$$\xi_a = (a - x_p) \left[\frac{\phi'''(x_p)}{2} \right]^{\frac{1}{3}} , \tag{2.27}$$

$$G_{s,h}(s) = f_{s,h}(x) \frac{dx}{ds} , \text{ and} \tag{2.28}$$

$$\frac{dx}{ds} = \left[\frac{2}{\phi'''(x_p)} \right]^{\frac{1}{3}} . \tag{2.29}$$

The proper branches for ξ_a and $\frac{dx}{ds}$ depend on the sign of $\phi'''(x_p)$, thus

$$\xi_a = \begin{cases} \pm|\xi_a|e^{j\frac{\pi}{3}} & \text{if } \phi'''(x_p) \leq 0 \\ \pm|\xi_a| & \text{if } \phi'''(x_p) > 0 \end{cases}, \quad \pm \text{ for } a \gtrless x_p, \text{ or} \tag{2.30}$$

$$|\xi_a| = |a - x_p| \left| \frac{\phi'''(x_p)}{2} \right|^{\frac{1}{3}} = |\phi'(a) - \phi'(x_p)|^{1/2} \left| \frac{2}{\phi'''(x_p)} \right|^{\frac{1}{6}} , \tag{2.31}$$

$$\frac{dx}{ds} = \begin{cases} \left|\frac{dx}{ds}\right| e^{-j\frac{\pi}{3}} & \text{if } \phi'''(x_p) \le 0 \\ \left|\frac{dx}{ds}\right| & \text{if } \phi'''(x_p) > 0 \end{cases}, \text{ and} \tag{2.32}$$

$$\left|\frac{dx}{ds}\right| = \left|\frac{2}{\phi'''(x_p)}\right|^{\frac{1}{3}}. \tag{2.33}$$

Next we employ the Chester et al. expansion [10] for the amplitude function in Equation (2.26), i.e.,

$$G_{s,h}(s) = \sum_{m=0}^{\infty} [a_m^{s,h}(s^2+\beta)^m + b_m^{s,h} s(s^2+\beta)^m] \tag{2.34}$$

and since only the leading terms in the asymptotic expansion of (2.26) will be retained, Equation (2.34) may be written as follows:

$$G_{s,h}(s) = a_0^{s,h} + s b_0^{s,h} + (s^2+\beta) g_{s,h}(s) \tag{2.35}$$

where

$$a_0^{s,h} = \frac{1}{2}[G_{s,h}(s_1) + G_{s,h}(s_2)], \tag{2.36}$$

$$b_0^{s,h} = \frac{1}{2s_1}[G_{s,h}(s_1) - G_{s,h}(s_2)], \text{ and} \tag{2.37}$$

$$g_{s,h}(s) = \sum_{m=1}^{\infty} [a_m^{s,h}(s^2+\beta)^{m-1} + b_m^{s,h} s(s^2+\beta)^{m-1}]. \tag{2.38}$$

Now, using the far-zone observation approximation and the symmetry of the surface near and around $s = 0$ or $x = x_p$, Equations (2.36) and (2.37) simplify as follows:

$$a_0^{s,h} \simeq G_{s,h}(s_{1,2}) = f_{s,h}(x_{1,2}) \left.\frac{dx}{ds}\right|_{s=s_{1,2}}, \text{ and} \tag{2.39}$$

$$b_0^{s,h} \simeq 0 \tag{2.40}$$

where

$$\left.\frac{dx}{ds}\right|_{s=s_{1,2}} = \sqrt{\frac{\tau''(s_{1,2})}{\phi''(x_{1,2})}} = \sqrt{\frac{\pm 2(-\beta)^{1/2}}{\phi''(x_{1,2})}}, \tag{2.41}$$

and using Equations (2.32), (2.33), (2.39), and (2.41) we have

$$a_0^{s,h} = \begin{cases} |a_0^{s,h}| e^{-j\frac{\pi}{3}} & \text{if } \phi'''(x_p) \le 0 \\ |a_0^{s,h}| & \text{if } \phi'''(x_p) > 0 \end{cases} \tag{2.42}$$

where

$$|a_0^{s,h}| = |f_{s,h}(x_{1,2})| \left| \frac{2\beta^{1/2}}{\phi''(x_{1,2})} \right|^{\frac{1}{2}} = |f_{s,h}(x_{1,2})| \left| \frac{2}{\phi'''(x_p)} \right|^{\frac{1}{3}} . \tag{2.43}$$

Then, using Equations (2.35) and (2.40) $e_{s,h}(\theta', \theta)$ may be given by the following expression:

$$e_{s,h}(\theta', \theta) = e^{jk\tau(0)} \left[a_0^{s,h} \int_{\xi_a}^{"\infty"} e^{jk(\beta s + s^3/3)}\, ds + \int_{\xi_a}^{"\infty"} (s^2 + \beta) g_{s,h}(s) e^{jk(\beta s + s^3/3)}\, ds \right] . \tag{2.44}$$

The integrand of the second integral on the right is regular over the entire path of integration, thus integration by parts yields

$$e_{s,h}(\theta', \theta) = e^{jk\tau(0)} \left[a_0^{s,h} \int_{\xi_a}^{"\infty"} e^{jk(\beta s + s^3/3)}\, ds - \frac{1}{jk} g_{s,h}(\xi_a) e^{jk(\beta \xi_a + \xi_a^3/3)} \right] + O(k^{-2}) \tag{2.45}$$

and using Equations (2.19) and (2.35) it simplifies further

$$e_{s,h}(\theta', \theta) \sim e^{jk\tau(0)} a_0^{s,h} \int_{\xi_a}^{"\infty"} e^{jk(\beta s + s^3/3)}\, ds + e^{jk\tau(\xi_a)} \left[\frac{a_0^{s,h}}{jk(\beta + \xi_a^2)} - \frac{G_{s,h}(\xi_a)}{jk\tau'(\xi_a)} \right] \tag{2.46}$$

where the terms of order higher than $1/k$ have been omitted. Next, we let $s = k^{-1/3}t$, $\beta = k^{-2/3}\tilde{\beta}$ and $\xi_a = k^{-1/3}\tilde{\xi}_a$ in (2.46), thus

$$e_{s,h}(\theta', \theta) \sim e^{jk\tau(0)} k^{-1/3} a_0^{s,h} \int_{\tilde{\xi}_a}^{"\infty"} e^{j(\tilde{\beta} t + t^3/3)}\, dt + e^{jk\tau(\xi_a)} \left[\frac{k^{-1/3} a_0^{s,h}}{j(\tilde{\beta} + \tilde{\xi}_a^{\,2})} - \frac{G_{s,h}(\xi_a)}{jk\tau'(\xi_a)} \right] . \tag{2.47}$$

Finally, the field angular dependence is given by the following expressions depending on the sign of $\phi'''(x_p)$ and $\phi'(x_p)$:

1. $\phi'''(x_p) \leq 0$ and $\phi'(x_p) \gtrless 0$

In this case, $\tilde{\beta} = \sigma e^{-j\frac{\pi}{3}}$, $\tilde{\xi}_a = \zeta_a e^{j\frac{\pi}{3}}$, $a_0^{s,h} = |a_0^{s,h}| e^{-j\frac{\pi}{3}}$ and Equation (2.47) becomes:

$$e_{s,h}(\theta', \theta) \sim e^{jk\phi(x_p)} k^{-\frac{1}{3}} |a_0^{s,h}| \overline{\mathrm{Ai}}^*(-\sigma, \zeta_a) + e^{jk\phi(a)} \left[\frac{k^{-\frac{1}{3}} |a_0^{s,h}|}{j(\sigma - \zeta_a^2)} + \frac{j}{k} \frac{f_{s,h}(a)}{\phi'(a)} \right] . \tag{2.48}$$

2. $\phi'''(x_p) \lesseqgtr 0$ and $\phi'(x_p) \gtrless 0$

In this case, $\tilde{\beta} = \sigma$, $\tilde{\xi}_a = \zeta_a$, $a_0^{s,h} = |a_0^{s,h}|$ and Equation (2.47) becomes:

$$e_{s,h}(\theta', \theta) \sim e^{jk\phi(x_p)} k^{-\frac{1}{3}} |a_0^{s,h}| \overline{\mathrm{Ai}}(\sigma, \zeta_a) + e^{jk\phi(a)} \left[\frac{k^{-\frac{1}{3}} |a_0^{s,h}|}{j(\sigma + \zeta_a^2)} + \frac{j}{k} \frac{f_{s,h}(a)}{\phi'(a)} \right] . \quad (2.49)$$

Both σ and ζ_a are real quantities with $\sigma \gtrless 0$ if $\phi'(x_p) \gtrless 0$ and $\zeta_a \gtrless 0$ if $a \gtrless x_p$. $\overline{\mathrm{Ai}}(\sigma, \gamma)$ is the incomplete Airy integral defined by:

$$\overline{\mathrm{Ai}}(\sigma, \gamma) \triangleq \int_{\gamma}^{\infty} e^{j(\sigma z + z^3/3)} \, dz \, . \quad (2.50)$$

2.2 Total Field Solution

Using Equations (2.10), (2.48) and (2.49), the total scattered field is given by:

1. $\phi'''(x_p) \leq 0$

$$\begin{aligned} U_z^s(\rho) \sim \mp \Bigg\{ & e^{jk\phi(x_p)} \frac{e^{j\frac{\pi}{4}} k^{\frac{1}{6}}}{\sqrt{2\pi}} |a_0^{s,h}| \overline{\mathrm{Ai}}^*(\sigma, \zeta_a) \\ & + e^{jk\phi(a)} \left[- \frac{k^{\frac{1}{6}} |a_0^{s,h}| e^{j\frac{\pi}{4}}}{j\sqrt{2\pi}(\sigma + \zeta_a^2)} - \frac{e^{-j\frac{\pi}{4}}}{\sqrt{2\pi k}} \frac{f_{s,h}(a)}{\phi'(a)} \right] \Bigg\} \frac{e^{-jk\rho}}{\sqrt{\rho}} \end{aligned} \quad (2.51)$$

with $\sigma \lesseqgtr 0$ if $\phi'(x_p) \gtrless 0$.

2. $\phi'''(x_p) > 0$

$$\begin{aligned} U_z^s(\rho) \sim \mp \Bigg\{ & e^{jk\phi(x_p)} \frac{e^{j\frac{\pi}{4}} k^{\frac{1}{6}}}{\sqrt{2\pi}} |a_0^{s,h}| \overline{\mathrm{Ai}}(\sigma, \zeta_a) \\ & + e^{jk\phi(a)} \left[\frac{k^{\frac{1}{6}} |a_0^{s,h}| e^{j\frac{\pi}{4}}}{j\sqrt{2\pi}(\sigma + \zeta_a^2)} - \frac{e^{-j\frac{\pi}{4}}}{\sqrt{2\pi k}} \frac{f_{s,h}(a)}{\phi'(a)} \right] \Bigg\} \frac{e^{-jk\rho}}{\sqrt{\rho}} \end{aligned} \quad (2.52)$$

with $\sigma \gtrless 0$ if $\phi'(x_p) \gtrless 0$.

The $\mp$ in front of the expressions in (2.51) and (2.52) corresponds to the soft or hard polarization cases. Notice that the last two terms in Equations (2.51) and (2.52)

are purely edge diffraction contributions where the first term in (2.51) and (2.52) appears to be a contribution from the zero-curvature point. In fact, three different scattering contributions, namely reflection, edge and zero-curvature diffraction are implicitly contained in the incomplete Airy integral. It is advantageous to separate the scattering mechanisms, extract the appropriate reflection and diffraction coefficients, and cast the total solution in a UTD format. In this form, the solution would be applicable to more general problems and also provide important physical insight into the individual scattering processes. The details of the separation procedure are presented in the next chapter.

Chapter 3

Extended UTD Solution Formulation

The total scattered field from the semi-infinite perfectly conducting cubic polynomial boundary of Figure 2.2 can be expressed as follows:

$$U_z^s(\rho) \simeq U_z^r(\rho) + U_z^c(\rho) + U_z^d(\rho) \tag{3.1}$$

where U_z^r, U_z^c and U_z^d are the reflected, zero-curvature and edge diffracted field components. Although additional higher-order mechanisms such as surface waves, double diffraction and whispering gallery modes may also exist, they will not be considered in this analysis since the PO approximation to the induced surface currents does not account for such effects. Before proceeding with the expressions for each field component, the various field contributions that are implicitly contained in the incomplete Airy integral are extracted by deforming the original contour of integration into appropriate steepest descent paths through the critical points of the integrand.

First, let's consider the complex plane topology of the incomplete Airy integral when the saddle points are real ($\sigma < 0$), as depicted in Figure 3.1. There exist three cases depending on the location of the endpoint γ relative to the saddle points z_1 and z_2, and $\overline{\mathrm{Ai}}(\sigma,\gamma)$ may be written as follows:

$$\overline{\mathrm{Ai}}(\sigma,\gamma) = \int_{\gamma}^{\infty \exp(j\psi_2)} e^{j(\sigma z + z^3/3)}\, dz + \int_{L_{23}} e^{j(\sigma z + z^3/3)}\, dz$$

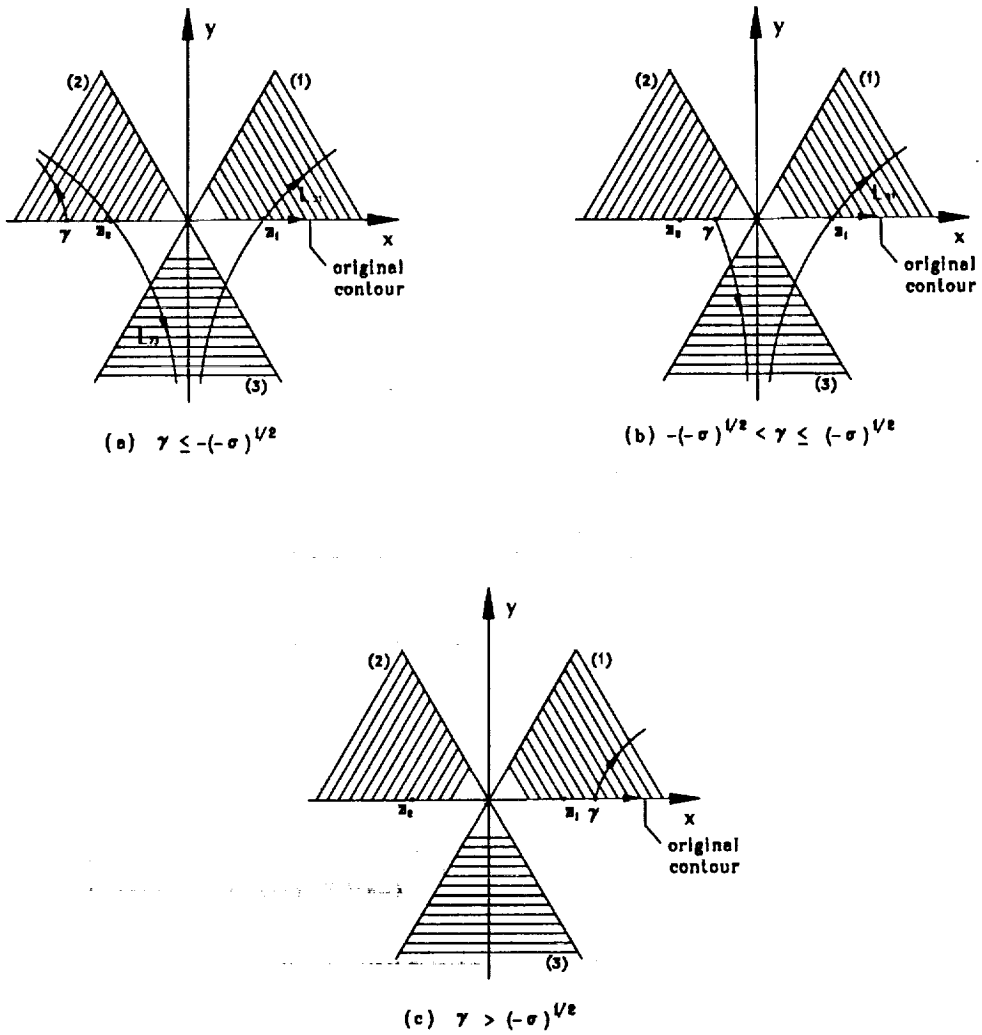

Figure 3.1: Complex plane topology and contour deformation for the incomplete Airy integral when $\sigma < 0$.

$$+ \int_{L_{31}} e^{j(\sigma z + z^3/3)}\, dz \quad \text{if } \gamma \le -(-\sigma)^{1/2}, \tag{3.2}$$

$$= \int_{\gamma}^{\infty \exp(j\psi_3)} e^{j(\sigma z + z^3/3)}\, dz + \int_{L_{31}} e^{j(\sigma z + z^3/3)}\, dz$$

$$\text{if } -(-\sigma)^{1/2} < \gamma \le (-\sigma)^{1/2}, \text{ and} \tag{3.3}$$

$$= \int_{\gamma}^{\infty \exp(j\psi_1)} e^{j(\sigma z + z^3/3)}\, dz \quad \text{if } \gamma > (-\sigma)^{1/2}. \tag{3.4}$$

Using the definitions for the ordinary and incomplete Airy functions found in Appendices A and B the integrals in (3.2)-(3.4) may be expressed in terms of these functions as follows:

$$\int_{\gamma}^{\infty \exp(j\psi_2)} e^{j(\sigma z + z^3/3)}\, dz = g_2(\sigma, \gamma), \tag{3.5}$$

$$\int_{L_{23}} e^{j(\sigma z + z^3/3)}\, dz = \pi[\mathrm{Ai}(\sigma) - j\mathrm{Bi}(\sigma)], \tag{3.6}$$

$$\int_{\gamma}^{\infty \exp(j\psi_3)} e^{j(\sigma z + z^3/3)}\, dz = g_3(\sigma, \gamma), \tag{3.7}$$

$$\int_{L_{31}} e^{j(\sigma z + z^3/3)}\, dz = \pi[\mathrm{Ai}(\sigma) + j\mathrm{Bi}(\sigma)], \text{ and} \tag{3.8}$$

$$\int_{\gamma}^{\infty \exp(j\psi_1)} e^{j(\sigma z + z^3/3)}\, dz = g_1(\sigma, \gamma). \tag{3.9}$$

Thus, using Equations (3.2)-(3.9), the total scattered field solution in (2.51) and (2.52) when $\sigma < 0$ (lit side of the caustic) is given by:

1. $\phi'''(x_p) \le 0$

$$\begin{aligned} U_z^s(\rho) \sim \mp \Bigg(\sqrt{\frac{\pi}{2}} e^{j\frac{\pi}{4}} k^{\frac{1}{6}} |a_0^{s,h}| \Big\{ & e^{jk\phi(x_1)}\, e^{-j\frac{2}{3}(-\sigma)^{3/2}} [\mathrm{Ai}^*(\sigma) - j\mathrm{Bi}^*(\sigma)] u[(-\sigma)^{1/2} - \zeta_a] \\ + \; & e^{jk\phi(x_2)}\, e^{j\frac{2}{3}(-\sigma)^{3/2}} [\mathrm{Ai}(\sigma) + j\mathrm{Bi}(\sigma)] u[-(-\sigma)^{1/2} - \zeta_a] \Big\} \\ + \; & e^{jk\phi(a)} \left\{ \frac{e^{j\frac{\pi}{4}} k^{\frac{1}{6}}}{\sqrt{2\pi}} |a_0^{s,h}| \left[\frac{j}{\sigma + \zeta_a^2} + e^{j(\sigma\zeta_a + \zeta_a^3/3)} I_l^*(\sigma, \zeta_a) \right] \right. \\ - \; & \left. \left. \frac{e^{-j\frac{\pi}{4}}}{\sqrt{2\pi k}} \frac{f_{s,h}(a)}{\phi'(a)} \right] \right\} \Bigg) \frac{e^{-jk\rho}}{\sqrt{\rho}} \end{aligned} \tag{3.10}$$

2. $\phi'''(x_p) > 0$

$$U_z^s(\rho) \sim \mp \left(\sqrt{\frac{\pi}{2}} e^{j\frac{\pi}{4}} k^{\frac{1}{6}} |a_0^{s,h}| \left\{ e^{jk\phi(x_1)}\, e^{j\frac{2}{3}(-\sigma)^{3/2}} [\mathrm{Ai}(\sigma) + j\mathrm{Bi}(\sigma)] u[(-\sigma)^{1/2} - \zeta_a] \right.\right.$$

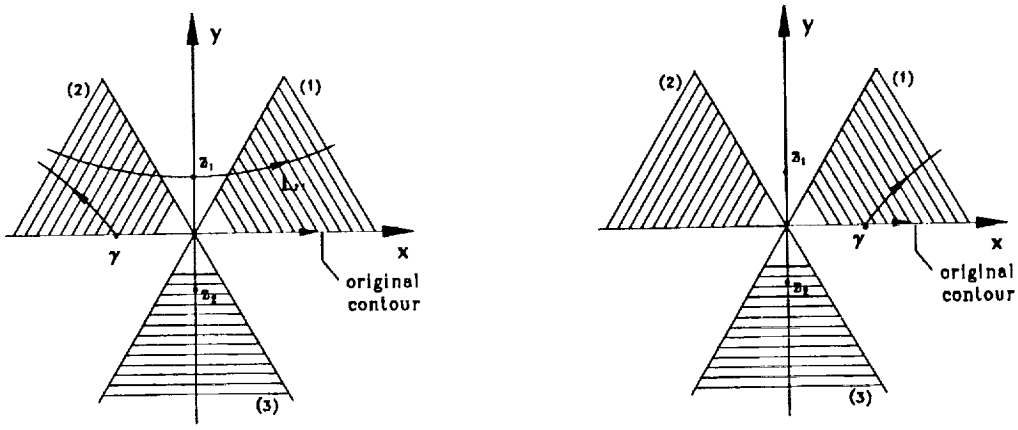

Figure 3.2: Complex plane topology and contour deformation for the incomplete Airy integral when $\sigma > 0$.

$$
\begin{aligned}
&+ \quad e^{jk\phi(x_2)}\, e^{-j\frac{2}{3}(-\sigma)^{3/2}} [\mathrm{Ai}^*(\sigma) - j\mathrm{Bi}^*(\sigma)] u[-(-\sigma)^{1/2} - \zeta_a] \Big\} \\
&+ \quad e^{jk\phi(a)} \left\{ \frac{e^{j\frac{\pi}{4}} k^{\frac{1}{6}}}{\sqrt{2\pi}} |a_0^{s,h}| \left[\frac{-j}{\sigma + \zeta_a^2} + e^{-j(\sigma\zeta_a + \zeta_a^3/3)} I_l(\sigma, \zeta_a) \right] \right. \\
&- \quad \left. \left. \frac{e^{-j\frac{\pi}{4}}}{\sqrt{2\pi k}} \frac{f_{s,h}(a)}{\phi'(a)} \right] \right\} \Big) \frac{e^{-jk\rho}}{\sqrt{\rho}}
\end{aligned}
\tag{3.11}
$$

where

$$
I_l(\sigma, \zeta) = \begin{cases} \mathrm{g}_2(\sigma, \zeta_a) & \text{if } \zeta_a \leq -(-\sigma)^{1/2} \\ \mathrm{g}_3(\sigma, \zeta_a) & \text{if } -(-\sigma)^{1/2} < \zeta_a \leq (-\sigma)^{1/2} \\ \mathrm{g}_1(\sigma, \zeta_a) & \text{if } \zeta_a > (-\sigma)^{1/2} \end{cases} \tag{3.12}
$$

and $u(x)$ is the Heaviside unit step function. The first two terms in Equations (3.10) and (3.11) represent uniform reflected field contributions where the last two terms represent edge diffraction contributions.

Next, let's consider the complex plane topology of $\overline{\mathrm{Ai}}(\sigma, \gamma)$ when the saddle points are complex ($\sigma > 0$), as depicted in Figure 3.2. There exist two cases depending on the endpoint location relative to the zero-curvature point ($z = 0$), and the incom-

plete Airy integral may be expressed in terms of the complete and incomplete Airy functions in a fashion similar to the previous case, i.e.,

$$\overline{\mathrm{Ai}}(\sigma,\gamma) = \mathrm{g}_2(\sigma,\gamma) + 2\pi\mathrm{Ai}(\sigma) \quad \text{if } \gamma \le 0, \text{ and} \tag{3.13}$$

$$= \mathrm{g}_1(\sigma,\gamma) \quad \text{if } \gamma > 0\,. \tag{3.14}$$

Then, using Equations (3.13) and (3.14), the total scattered field of (2.51) and (2.52) when $\sigma > 0$ (dark side of the caustic) is given by:

1. $\phi'''(x_p) \le 0$

$$\begin{aligned} U_z^s(\rho) \sim & \mp \left(e^{jk\phi(x_p)}\sqrt{2\pi}e^{j\frac{\pi}{4}}k^{\frac{1}{6}}|a_0^{s,h}|\mathrm{Ai}^*(\sigma)u(-\zeta_a) \right. \\ & + e^{jk\phi(a)} \left\{ \frac{e^{j\frac{\pi}{4}}k^{\frac{1}{6}}}{\sqrt{2\pi}}|a_0^{s,h}| \left[\frac{j}{\sigma+\zeta_a^2} + e^{j(\sigma\zeta_a+\zeta_a^3/3)} I_d^*(\sigma,\zeta_a) \right] \right. \\ & \left. \left. - \frac{e^{-j\frac{\pi}{4}}}{\sqrt{2\pi k}} \frac{f_{s,h}(a)}{\phi'(a)} \right] \right\} \Bigg) \frac{e^{-jk\rho}}{\sqrt{\rho}} \end{aligned} \tag{3.15}$$

2. $\phi'''(x_p) > 0$

$$\begin{aligned} U_z^s(\rho) \sim & \mp \left(e^{jk\phi(x_p)}\sqrt{2\pi}e^{j\frac{\pi}{4}}k^{\frac{1}{6}}|a_0^{s,h}|\mathrm{Ai}(\sigma)u(-\zeta_a) \right. \\ & + e^{jk\phi(a)} \left\{ \frac{e^{j\frac{\pi}{4}}k^{\frac{1}{6}}}{\sqrt{2\pi}}|a_0^{s,h}| \left[\frac{-j}{\sigma+\zeta_a^2} + e^{-j(\sigma\zeta_a+\zeta_a^3/3)} I_d(\sigma,\zeta_a) \right] \right. \\ & \left. \left. - \frac{e^{-j\frac{\pi}{4}}}{\sqrt{2\pi k}} \frac{f_{s,h}(a)}{\phi'(a)} \right] \right\} \Bigg) \frac{e^{-jk\rho}}{\sqrt{\rho}} \end{aligned} \tag{3.16}$$

where

$$I_d(\sigma,\zeta) = \begin{cases} \mathrm{g}_2(\sigma,\zeta_a) & \text{if } \zeta_a \le 0 \\ \mathrm{g}_1(\sigma,\zeta_a) & \text{otherwise} \end{cases}\,. \tag{3.17}$$

In this case the first term in Equations (3.15) and Equation (3.16) represent zero-curvature diffraction contribution where the last two terms in (3.15) and (3.16) represent edge diffraction contributions. Notice that the zero-curvature diffraction contribution is a uniform version of the complex ray (evanescent) field interpretation of Ikuno and Felsen [11, 12], and it appropriately reduces to their expressions when

$\sigma \gg 1$. The main advantage of our formulation is of course uniformity, and also the need for a complex extension of the reflecting boundary and the evaluation of surface parameters in complex space is avoided.

Another observation concerning the edge diffracted field component of the total field is that the last term in Equations (3.10), (3.11), (3.15) and (3.16) can be recognized as the PO half-plane diffraction coefficient, and using the following expressions:

$$f_{s,h}(a) = h(a)\hat{n}'(Q'_a) \cdot \left\{ \begin{array}{c} \hat{s}^i \\ \\ \hat{s} \end{array} \right\} = h(a) \left\{ \begin{array}{c} \sin\varphi' \\ \\ \sin\varphi \end{array} \right\} \tag{3.18}$$

$$\phi'(a) = h(a)\hat{t}'(Q'_a) \cdot (\hat{s}^i + \hat{s}) = h(a)C(\varphi', \varphi) \tag{3.19}$$

it may be written as follows:

$$D^{PO}_{s,h}(\varphi', \varphi) = \pm \frac{e^{-j\frac{\pi}{4}}}{\sqrt{2\pi k}} \frac{(\sin\varphi' \, ; \, \sin\varphi)}{(\cos\varphi' + \cos\varphi)} \tag{3.20}$$

where φ' and φ are the angles of incidence and observation, respectively, measured from the edge-fixed coordinate system. It is well known that the PO diffraction coefficient does not satisfy reciprocity nor does it satisfy the local boundary condition on the surface for the TM polarization case. These shortcomings produce errors in the total scattered field for observation points away from the optical boundaries. A rigorous method of providing the necessary corrections to the PO approximation involves the introduction of an additional non-uniform induced current near the edge. A rather heuristic but simpler approach for improving the PO half-plane diffraction coefficient is to introduce a pair of edge correction multiplication terms derived by James [13], i.e.,

$$C_s(\varphi', \varphi) = \sin(\varphi/2) \sec(\varphi'/2), \text{ and} \tag{3.21}$$

$$C_h(\varphi', \varphi) = \cos(\varphi'/2) \csc(\varphi/2) \tag{3.22}$$

which correct the PO diffraction coefficient so that it yields the exact diffraction coefficient outside the optical boundaries. These correction factors reduce to zero

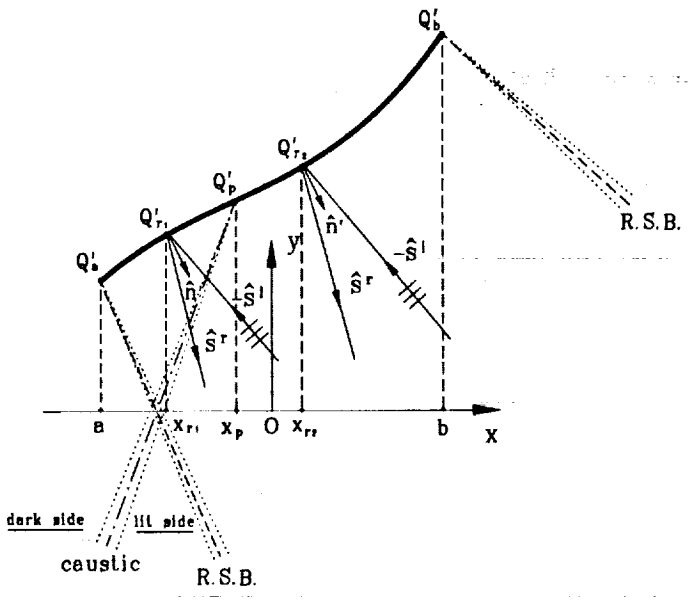

Figure 3.3: Geometry for the reflected field from a cubic polynomial strip.

near the optical boundaries, and therefore they do not affect the cancellation of singularities or the compensation of discontinuities in the reflected field components.

A final comment about the total field solution in Equations (3.10), (3.11), (3.15), and (3.16) is that it remains valid for any value of the cubic polynomial coefficients a_0, a_1, a_2, and a_3 and one can show by carefully taking the appropriate limits that it reduces to the half-plane solution when a_2 and a_3 go to zero, and also reduces to the solution for a semi-infinite parabolic screen when a_3 goes to zero.

We are now ready to derive expressions for the individual scattered field contributions from a finite cubic polynomial surface using the expression for the total field from the semi-infinite surface given in (3.10), (3.11), (3.15) and (3.16) and by expressing the quantities $a_0^{s,h}$, σ and ζ_a in terms of the local surface parameters relevant to each scattering mechanism.

3.1 Reflected Field Solution

The geometry for the reflected field appears in Figure 3.3. The reflected field con-

tribution consists of two specular components that only exist in the lit side of the caustic. It is given by the following expression:

$$U_z^r(\rho) \sim U_z^{r_1}(\rho)u(b - x_{r_1}) + U_z^{r_2}(\rho)u(x_{r_2} - a) \tag{3.23}$$

where $U_z^{r_{1,2}}(\rho)$ are the two specular contributions given by

$$U_z^{r_{1,2}}(\rho) \sim e^{jk\vec{r}'(Q'_{r_{1,2}})\cdot\hat{s}^i}\mathcal{R}_{s,h}(Q'_{r_{1,2}})\sqrt{\frac{1}{2}R_g(Q'_{r_{1,2}})\hat{n}'(Q'_{r_{1,2}})\cdot\hat{s}^i}\, e^{jk\vec{r}'(Q'_{r_{1,2}})\cdot\hat{s}^r}\,\frac{e^{-jk\rho}}{\sqrt{\rho}} \tag{3.24}$$

$R_g(Q'_{r_i})$ is the principal radius of curvature at the reflection point given by

$$R_g(Q'_{r_i}) = \frac{h^3(x_{r_i})}{y''(x_{r_i})} \tag{3.25}$$

and $x_{r_{1,2}}$ are the specular points found by

$$x_{r_{1,2}} = \frac{-\bar{a}_2 \pm \sqrt{\bar{a}_2^2 - 4\bar{a}_3\bar{a}_1}}{2\bar{a}_3} \tag{3.26}$$

where

$$\bar{a}_1 = \hat{x}\cdot(\hat{s}^i + \hat{s}^r) + a_1\hat{y}\cdot(\hat{s}^i + \hat{s}^r) = C(\theta',\theta) + a_1 S(\theta',\theta)\,, \tag{3.27}$$

$$\bar{a}_2 = 2a_2\hat{y}\cdot(\hat{s}^i + \hat{s}^r) = 2a_2 S(\theta',\theta)\,, \quad \text{and} \tag{3.28}$$

$$\bar{a}_3 = 3a_3\hat{y}\cdot(\hat{s}^i + \hat{s}^r) = 3a_3 S(\theta',\theta)\,. \tag{3.29}$$

The quantity $\mathcal{R}_{s,h}(Q'_{r_i})$ is the uniform acoustic soft or hard reflection coefficient that remains valid as $Q'_{r_i} \to Q'_p$ and is given by

$$\mathcal{R}_{s,h}(Q'_{r_i}) = R_{s,h}\begin{cases} T_r(\sigma_r) & \text{if } R_g(Q'_{r_i}) \geq 0 \\ T_r^*(\sigma_r) & \text{if } R_g(Q'_{r_i}) < 0 \end{cases} \tag{3.30}$$

where

$$R_{s,h} = \mp 1\,, \text{ for a perfectly conducting boundary,} \tag{3.31}$$

$$T_r(\sigma_r) = \sqrt{\pi}\sigma_r^{1/4}e^{-j\frac{\pi}{4}}e^{-j\frac{2}{3}\sigma_r^{3/2}}[\mathrm{Ai}(-\sigma_r) - j\mathrm{Bi}(-\sigma_r)]\,, \quad \text{and} \tag{3.32}$$

$$\sigma_r = \left|\frac{3}{2}k[\vec{r}'(Q'_{r_i}) - \vec{r}'(Q'_p)]\cdot(\hat{s}^i + \hat{s}^r)\right|^{\frac{2}{3}}\,. \tag{3.33}$$

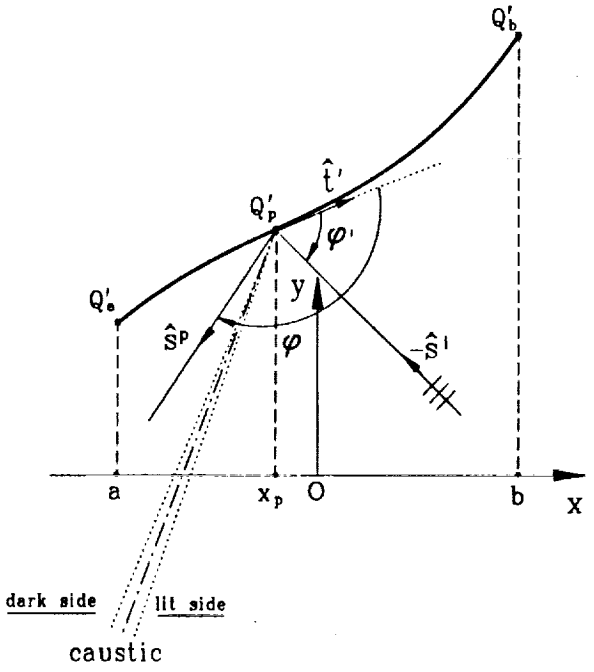

Figure 3.4: Geometry for the zero-curvature diffracted field from a cubic polynomial strip.

The quantity $T_r(\sigma_r)$ is the appropriate transition function that cancels the GO field singularity at the caustic. Also, when the specular point is far removed from the zero-curvature point (observation in the deep lit side of the caustic), $\sigma_r \gg 1$ and using the large negative argument forms of the ordinary Airy functions (see Appendix A) we have that $T_r(\sigma_r \gg 1) \sim 1$ and $\mathcal{R}_{s,h} \rightarrow R_{s,h}$ so that the extended UTD reflected field solution of Equation (3.24) reduces to the usual GO expression for the reflected field.

3.2 Zero-Curvature Diffracted Field Solution

The geometry for the zero curvature diffracted field is shown in Figure 3.4. The zero-curvature diffracted field contribution exists only in the dark side of the caustic

and compensates the reflected field discontinuity. It is given by

$$U_z^r(\rho) \sim e^{jk\vec{r}'(Q_p')\cdot\hat{s}^i} \mathcal{D}_{s,h}^r(Q_p') e^{jk\vec{r}'(Q_p')\cdot\hat{s}^p} \frac{e^{-jk\rho}}{\sqrt{\rho}} u(x_p - a)u(b - x_p) \tag{3.34}$$

where $\mathcal{D}_{s,h}^r(Q_p')$ is the scalar zero-curvature diffraction coefficient and is given by

$$\mathcal{D}_{s,h}^r(Q_p') = \mp\sqrt{2\pi} e^{j\frac{\pi}{4}} k^{\frac{1}{6}} \left|\frac{2}{y'''(x_p)}\right|^{\frac{1}{3}} L_c(\varphi', \varphi)\mathrm{Ai}(\sigma_c) \tag{3.35}$$

where

$$L_c(\varphi', \varphi) = \frac{\sqrt{S^2(\varphi', \varphi) + C^2(\varphi', \varphi)}}{|c_1 C(\varphi', \varphi) - c_2 S(\varphi', \varphi)|^{1/3}} \left|\cos\left(\frac{\varphi' - \varphi}{2}\right)\right| \tag{3.36}$$

$$\text{with} \quad c_1 = \frac{y'(x_p)}{h(x_p)} \quad \text{and} \quad c_2 = \frac{1}{h(x_p)}$$

is the diffraction coefficient angular dependance, and

$$\sigma_c = k^{\frac{2}{3}} \left|\frac{2}{y'''(x_p)}\right|^{\frac{1}{3}} \frac{|C(\varphi', \varphi)|}{c_2 |c_1 C(\varphi', \varphi) - c_2 S(\varphi', \varphi)|^{1/3}}. \tag{3.37}$$

Notice that the zero-curvature diffraction contribution is significant near the caustic and decays exponentially away from the caustic as $\mathrm{Ai}(\sigma_c \gg 1) \to 0$.

3.3 First-Order Edge Diffracted Field Solution

The geometry for the edge diffracted field is illustrated in Figure 3.5. The edge diffracted field contribution consists of two components (one from each of the two edges) and is given by

$$U_z^d(\rho) = U_z^{d_a}(\rho) + U_z^{d_b}(\rho) \tag{3.38}$$

where

$$U_z^{d_{a,b}}(\rho) \sim e^{jk\vec{r}'(Q_{a,b}')\cdot\hat{s}^i} \mathcal{D}_{s,h}^r(Q_{a,b}') e^{jk\vec{r}'(Q_{a,b}')\cdot\hat{s}^d} \frac{e^{-jk\rho}}{\sqrt{\rho}} \tag{3.39}$$

and $\mathcal{D}_{s,h}^r(Q_{a,b}')$ is the scalar uniform edge diffraction coefficient that remains valid as $Q_{a,b}' \to Q_p'$. It is comprised of two parts, i.e.,

$$\mathcal{D}_{s,h}^r(Q_{a,b}') = D_{s,h}^{hp}(Q_{a,b}') + D_{s,h}^r(Q_{a,b}') \tag{3.40}$$

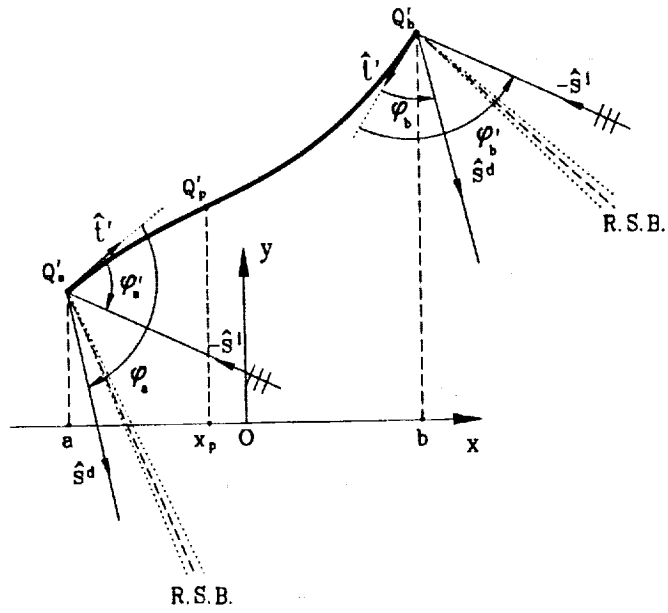

Figure 3.5: Geometry for the edge diffracted field from a cubic polynomial strip.

where $D^{hp}_{s,h}(Q'_{a,b})$ is the half-plane diffraction coefficient given by

$$D^{hp}_{s,h}(Q'_{a,b}) = \frac{-e^{-j\frac{\pi}{4}}}{2\sqrt{2\pi k}}\left[\sec\left(\frac{\varphi'_{a,b}-\varphi_{a,b}}{2}\right) \mp \sec\left(\frac{\varphi'_{a,b}+\varphi_{a,b}}{2}\right)\right] \tag{3.41}$$

and $D^{r}_{s,h}(Q'_{a,b})$ is a term that provides curvature correction and is given by

$$D^{r}_{s,h}(Q'_{a,b}) = \mp\frac{d_{a,b}k^{\frac{1}{6}}e^{j\frac{\pi}{4}}}{\sqrt{2\pi}}\left|\frac{2}{y'''(a,b)}\right|^{\frac{1}{3}} L_d(\varphi'_{a,b},\varphi_{a,b})\begin{cases} T_d(\sigma_{a,b},\zeta_{a,b}) & \text{if } y'''(a,b)\hat{y}\cdot(\hat{s}^i+\hat{s}^d)\le 0 \\ T^*_d(\sigma_{a,b},\zeta_{a,b}) & \text{if } y'''(a,b)\hat{y}\cdot(\hat{s}^i+\hat{s}^d)>0 \end{cases} \tag{3.42}$$

where

$$L_d(\varphi'_{a,b},\varphi_{a,b}) = \frac{\sqrt{C^2(\varphi'_{a,b},\varphi_{a,b})+S^2(\varphi'_{a,b},\varphi_{a,b})}}{|d_1C(\varphi'_{a,b},\varphi_{a,b})-d_2S(\varphi'_{a,b},\varphi_{a,b})|^{1/3}}\left|\cos\left(\frac{\varphi'_{a,b}-\varphi_{a,b}}{2}\right)\right| \tag{3.43}$$

$$T_d(\sigma,|\zeta|) = \frac{j}{\sigma+|\zeta|^2}+e^{j(\sigma|\zeta|+|\zeta|^3/3)}\begin{cases} g^*_3(\sigma,|\zeta|) & \text{if } \sigma+|\zeta|^2\le 0 \\ g^*_1(\sigma,|\zeta|) & \text{if } \sigma+|\zeta|^2>0 \end{cases}, \tag{3.44}$$

$$T_d(\sigma,-|\zeta|) = -T^*_d(\sigma,|\zeta|), \tag{3.45}$$

$$\sigma_{a,b} = k^{\frac{2}{3}}\left|\frac{2}{y'''(a,b)}\right|^{\frac{1}{3}}\frac{|d_3C(\varphi'_{a,b},\varphi_{a,b})+d_4S(\varphi'_{a,b},\varphi_{a,b})|}{|d_1C(\varphi'_{a,b},\varphi_{a,b})-d_2S(\varphi'_{a,b},\varphi_{a,b})|^{1/3}}\cdot \operatorname{sgn}\left[\frac{\hat{x}\cdot(\hat{s}^i+\hat{s}^d)+y'(x_p)\hat{y}\cdot(\hat{s}^i+\hat{s}^d)}{y'''(a,b)\hat{y}\cdot(\hat{s}^i+\hat{s}^d)}\right], \tag{3.46}$$

$$\zeta_{a,b} = \pm k^{\frac{1}{3}} |y'(a,b) - y'(x_p)|^{1/2} \left| \frac{2}{y'''(a,b)} \right|^{\frac{1}{6}} \cdot$$
$$|d_1 C(\varphi'_{a,b}, \varphi_{a,b}) - d_2 S(\varphi'_{a,b}, \varphi_{a,b})|^{\frac{1}{3}} \; ; \quad a, b \gtrless x_p \,, \tag{3.47}$$

$$d_{a,b} = \pm 1 \,, \tag{3.48}$$

$$d_1 = \pm \frac{y'(a,b)}{h(a,b)} \,, \tag{3.49}$$

$$d_2 = \frac{1}{h(a,b)} \,, \tag{3.50}$$

$$d_3 = \pm \frac{1 + y'(a,b)y'(x_p)}{h(a,b)} \,, \quad \text{and} \tag{3.51}$$

$$d_4 = \frac{y'(a,b) - y'(x_p)}{h(a,b)} \,. \tag{3.52}$$

Notice that the curvature correction part of the uniform edge diffraction coefficient in Equation (3.40) provides significant contribution near the reflection shadow boundary (RSB) where $\sigma + \zeta^2 \approx 0$. In fact both the half-plane and curvature components in (3.40) become singular near the RSB, however these singularities cancel each other out and the total diffraction coefficient remains finite. Away from the RSB ($\sigma + \zeta^2 \gg 0$) the curvature correction component reduces to zero as the diffraction transition function $T_d(\sigma, \zeta) \to 0$, and thus the edge diffraction solution reduces to the half-plane solution as it should.

Chapter 4

Numerical Results and Discussion

In this chapter, some numerical results for the scattered fields from a general cubic polynomial strip are presented. The scattering geometry and the relevant parameters are illustrated in Figure 4.1. The accuracy of the extended UTD solution is verified via comparison with method of moments results. Also, some results obtained using classic UTD are shown and illustrate the need for the new solution.

The first example considered is a cubic polynomial strip with $a_0 = 2.0\lambda$, $a_1 = 0.5$, $a_2 = 0.1\lambda^{-1}$, $a_3 = 0.1\lambda^{-2}$, $a = -1.5\lambda$, and $b = 1.5\lambda$. In this case both edges are far removed from the zero-curvature point and thus the two reflection shadow boundaries and the caustic of the reflected rays are clearly distinct. Figure 4.2 shows a plot of the magnitude of the various field contributions to the total field for the TM polarization case and an angle of incidence $\theta' = -45°$. Notice that the reflected field component exhibits a total of three discontinuities. The first discontinuity occurs across the caustic of the reflected rays at $\theta \approx -82°$ and is compensated by the zero-curvature diffracted field. The second discontinuity occurs at the RSB associated with the edge Q_a at $\theta \approx -50°$ and is compensated by the edge diffracted field from Q_a. Similarly the third discontinuity occurs at the RSB associated with the edge Q_b at $\theta \approx -23°$ and is compensated by the edge diffracted field from Q_b. Also notice that the two edge diffraction terms become singular near the incidence shadow boundary (ISB) at $\theta = 135°$; however, they combine to give a finite result.

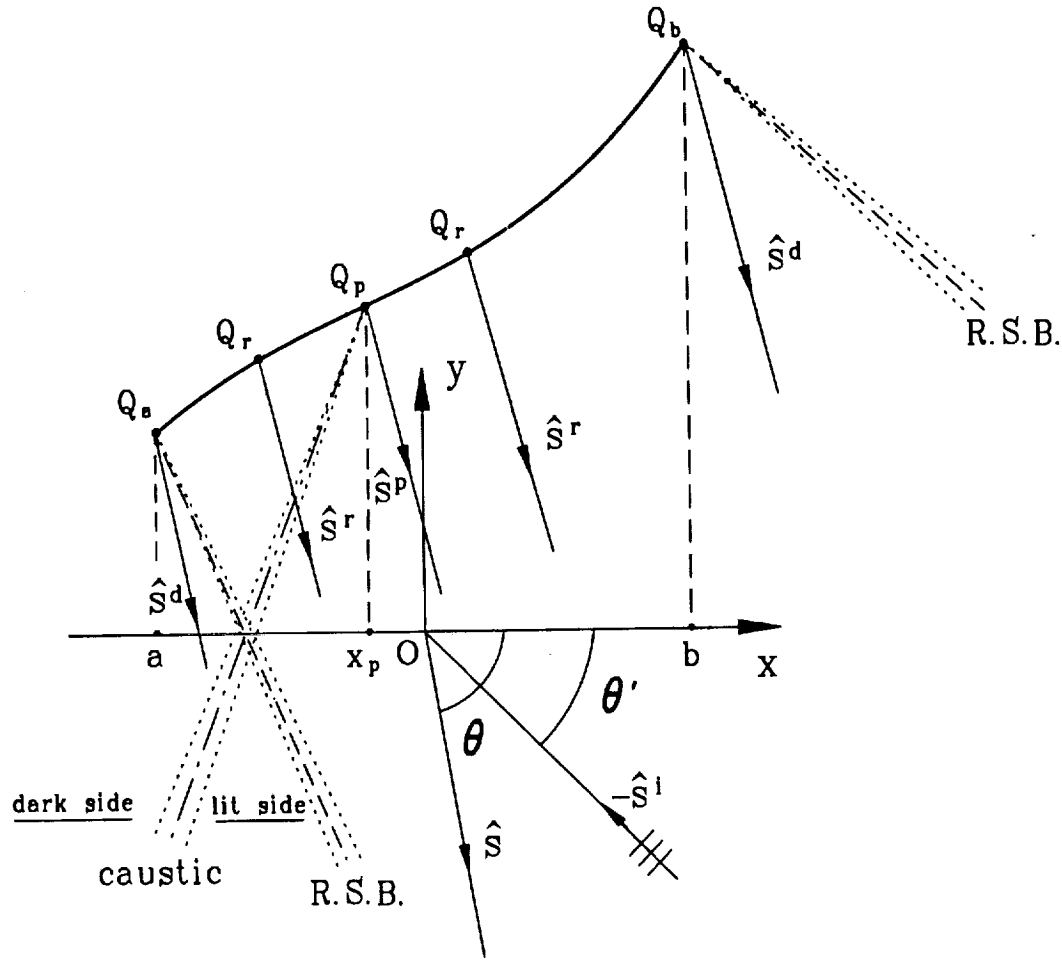

$$Y(x) = a_0 + a_1 x + a_2 x^2 + a_3 x^3 \; ; \quad a \leq x \leq b$$

Figure 4.1: Scattering geometry and relevant parameters for the numerical results.

Figure 4.3 shows a plot for the total scattered field in terms of bistatic echo width for the TM polarization. The extended UTD result shows excellent agreement with the method of moments where classic UTD gives an erroneous result near the caustic at $\theta \approx -82°$, and in both the lit and dark sides. This is expected since the classic UTD formulation does not contain zero-curvature diffraction information in the dark side and also uses the non-uniform GO expression for the reflected field contribution in the lit side. Figure 4.4 shows results for the bistatic echo width for the TE polarization. Again the extended UTD result shows good agreement with method of moments. The discrepancies for observation directions near grazing are attributed to higher order mechanisms missing from the total field. These higher order effects such as edge exited surface rays and whispering gallery modes are stronger for this polarization since the grazing fields do not vanish on the boundary as is the case for the TM polarization. The failure of the classic UTD near the caustic is again clearly illustrated. Figures 4.5 and 4.6 show plots of the monostatic echo width for the TM and TE polarizations, respectively. The extended UTD solution gives accurate results for the monostatic case also, except for the regions where the higher order mechanisms become significant. Contrary to the classic UTD result, the extended UTD solution remains finite and continuous across the caustics.

For the second example we consider a cubic polynomial strip with $a_0 = 2.0\lambda$, $a_1 = 0.5$, $a_2 = 0.1\lambda^{-1}$, $a_3 = 0.1\lambda^{-2}$, $a = -0.33\lambda$, and $b = 1.5\lambda$. In this case, the edge Q_a coincides with the zero-curvature point Q_p and thus the RSB and the caustic of the reflected rays coalesce to form a composite shadow boundary. Figure 4.7 shows a plot of the bistatic echo width for the TM polarization and an angle of incidence $\theta' = -45°$. The classic UTD result exhibits a singularity at the RSB associated with edge Q_a, where the extended UTD result remains finite and is in excellent agreement with the reference solution. Figure 4.8 shows a plot of the monostatic echo width for the same geometry. Again the non-uniformity of the classic UTD solution is clearly

evident where the extended UTD solution remains valid across the RSB and reduces to the classic UTD result away from the transition region.

The remaining two examples illustrate the universal nature of the extended UTD solution. For the third example we consider a cubic polynomial strip with $a_0 = 2.0\lambda$, $a_1 = 0.5$, $a_2 = 0.1\lambda^{-1}$, $a_3 = 0.0\lambda^{-2}$, $a = -0.33\lambda$, and $b = 1.5\lambda$. This of course corresponds to a parabolic screen and is well known that classic UTD gives accurate results. In this case the zero-curvature point theoretically moves to negative infinity. Figure 4.9 shows a plot of the monostatic echo width for the TM polarization and the extended UTD solution remains valid and shows excellent agreement with the reference solution.

For the final example we consider a flat strip by letting both the quadratic and cubic coefficients go to zero. Figure 4.10 shows a plot of the bistatic echo width for the TM polarization and an angle of incidence $\theta' = -45°$. The extended UTD solution remains valid for this special case also, and clearly demonstrates its flexibility for treating general surfaces that are highly curved, slightly curved, or completely flat.

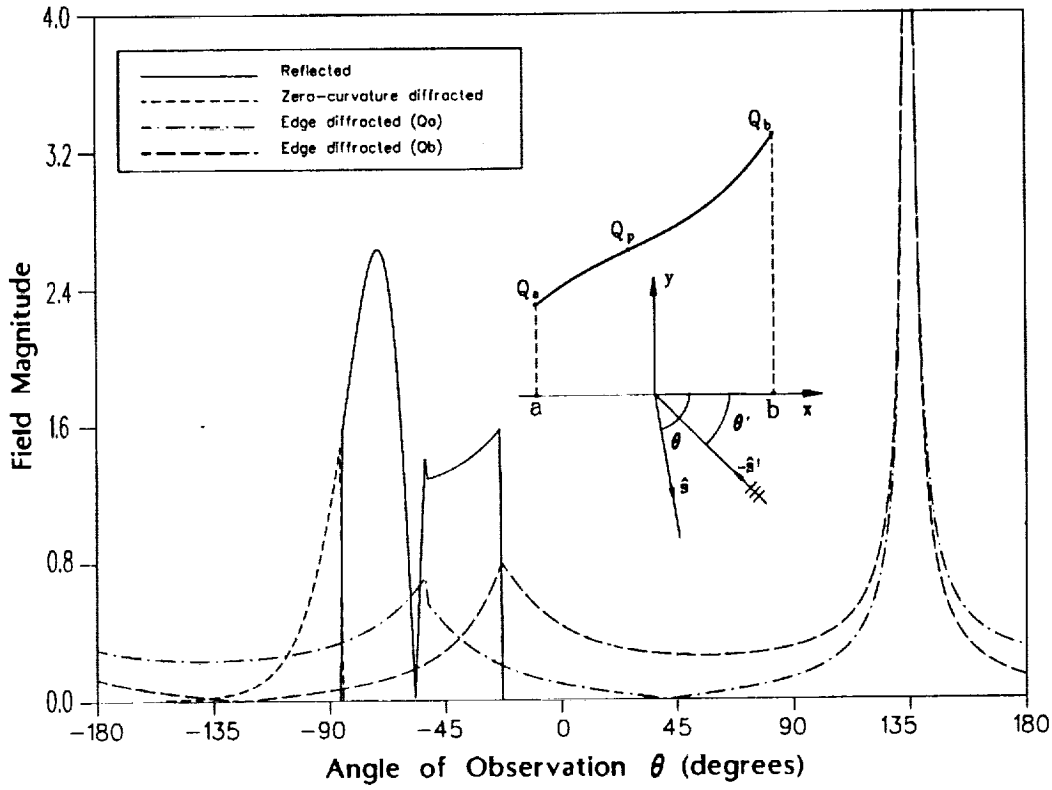

Figure 4.2: Scattered field contributions (TM polarization case) from a cubic polynomial strip with $a_0 = 2.0\lambda$, $a_1 = 0.5$, $a_2 = 0.1\lambda^{-1}$, $a_3 = 0.1\lambda^{-2}$, $a = -1.5\lambda$, $b = 1.5\lambda$, and angle of incidence $\theta' = -45°$.

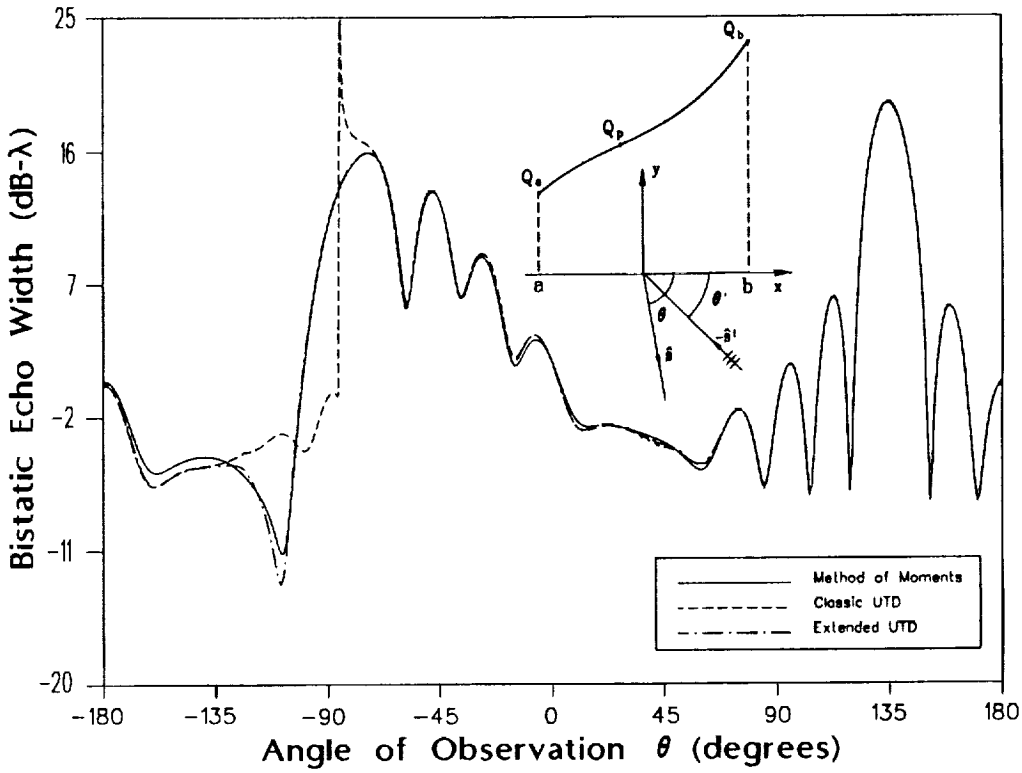

Figure 4.3: Bistatic echo width (TM polarization case) from a cubic polynomial strip with $a_0 = 2.0\lambda$, $a_1 = 0.5$, $a_2 = 0.1\lambda^{-1}$, $a_3 = 0.1\lambda^{-2}$, $a = -1.5\lambda$, $b = 1.5\lambda$, and angle of incidence $\theta' = -45°$.

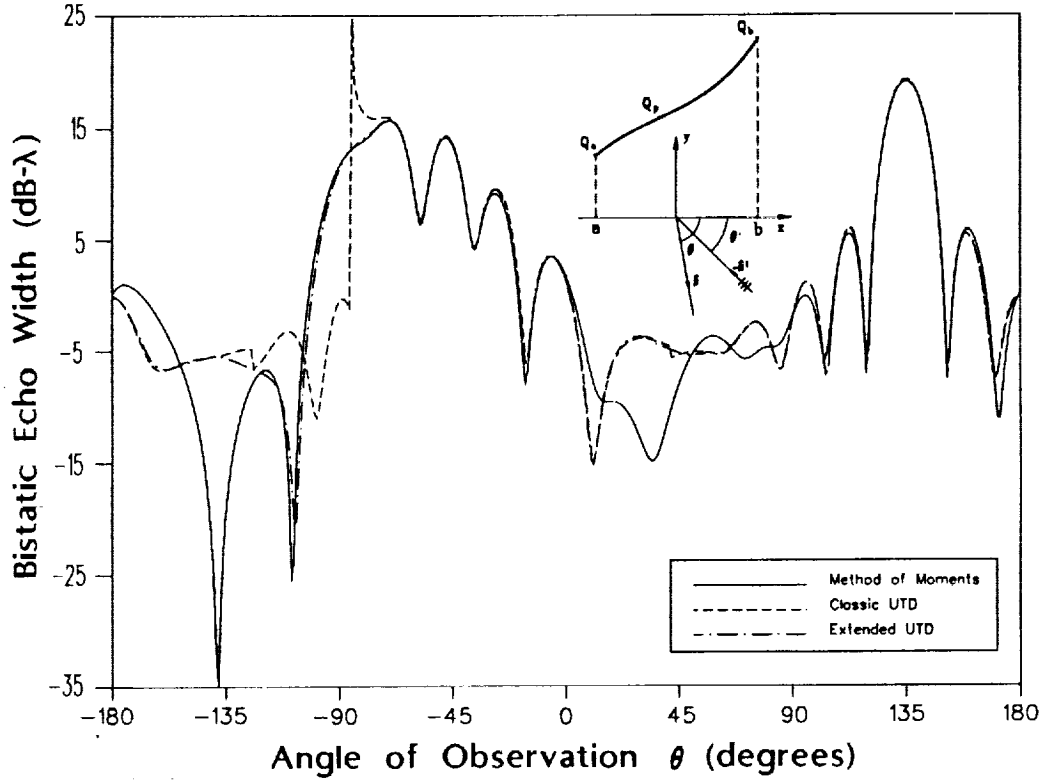

Figure 4.4: Bistatic echo width (TE polarization case) from a cubic polynomial strip with $a_0 = 2.0\lambda$, $a_1 = 0.5$, $a_2 = 0.1\lambda^{-1}$, $a_3 = 0.1\lambda^{-2}$, $a = -1.5\lambda$, $b = 1.5\lambda$, and angle of incidence $\theta' = -45°$.

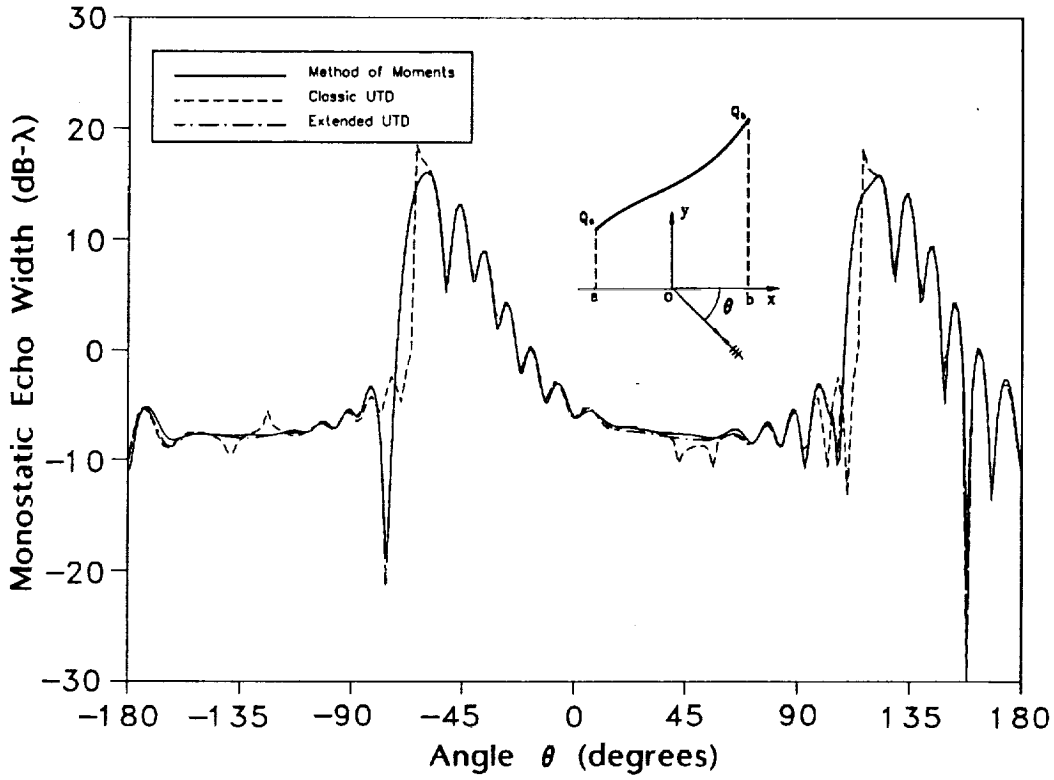

Figure 4.5: Monostatic echo width (TM polarization case) from a cubic polynomial strip with $a_0 = 2.0\lambda$, $a_1 = 0.5$, $a_2 = 0.1\lambda^{-1}$, $a_3 = 0.1\lambda^{-2}$, $a = -1.5\lambda$, and $b = 1.5\lambda$.

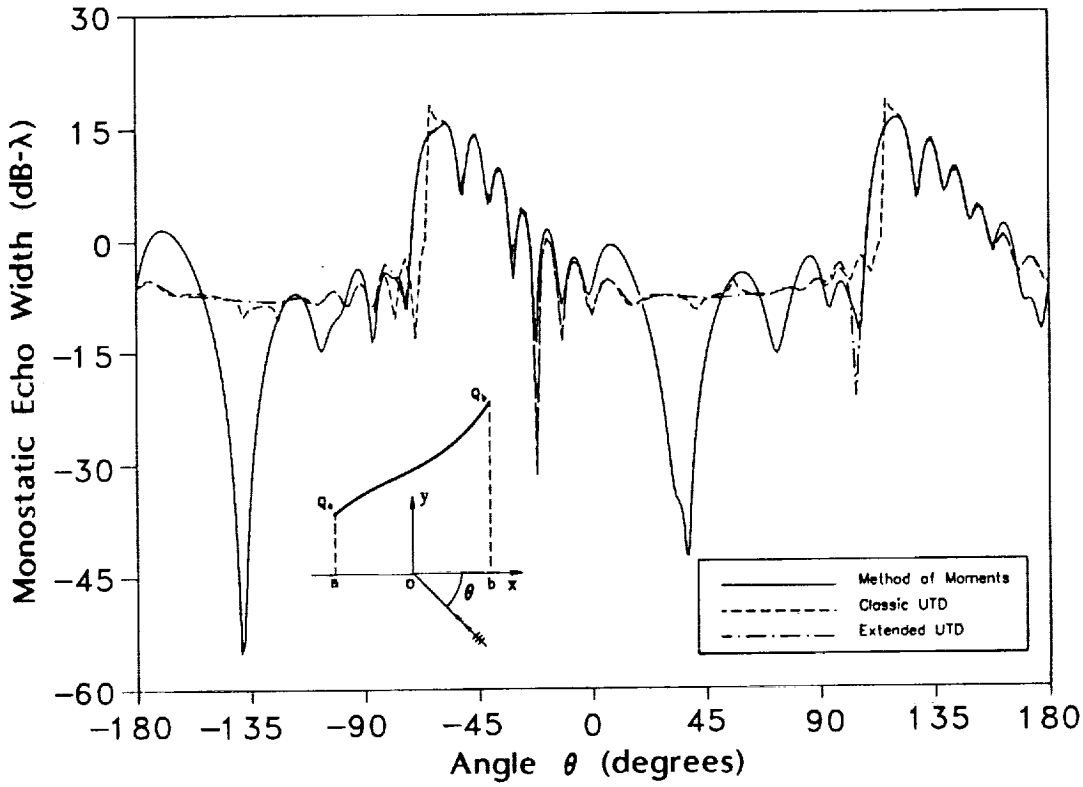

Figure 4.6: Monostatic echo width (TE polarization case) from a cubic polynomial strip with $a_0 = 2.0\lambda$, $a_1 = 0.5$, $a_2 = 0.1\lambda^{-1}$, $a_3 = 0.1\lambda^{-2}$, $a = -1.5\lambda$, and $b = 1.5\lambda$.

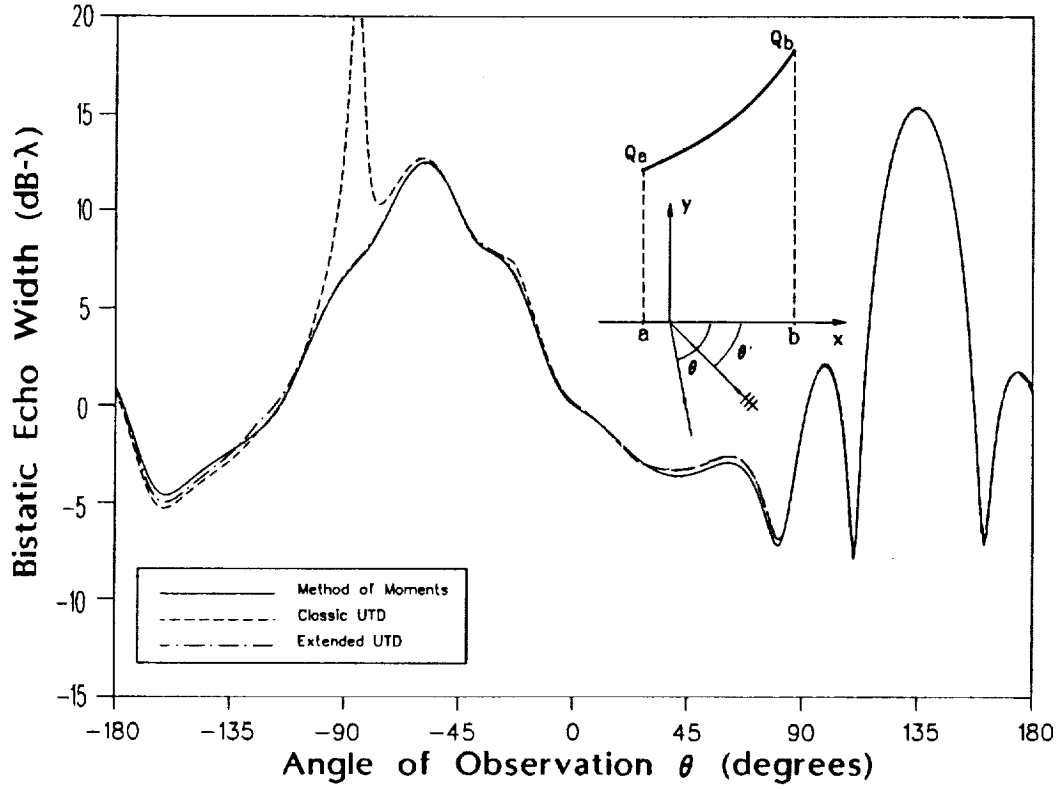

Figure 4.7: Bistatic echo width (TM polarization case) from a cubic polynomial strip with $a_0 = 2.0\lambda$, $a_1 = 0.5$, $a_2 = 0.1\lambda^{-1}$, $a_3 = 0.1\lambda^{-2}$, $a = -0.33\lambda$, $b = 1.5\lambda$, and angle of incidence $\theta' = -45°$.

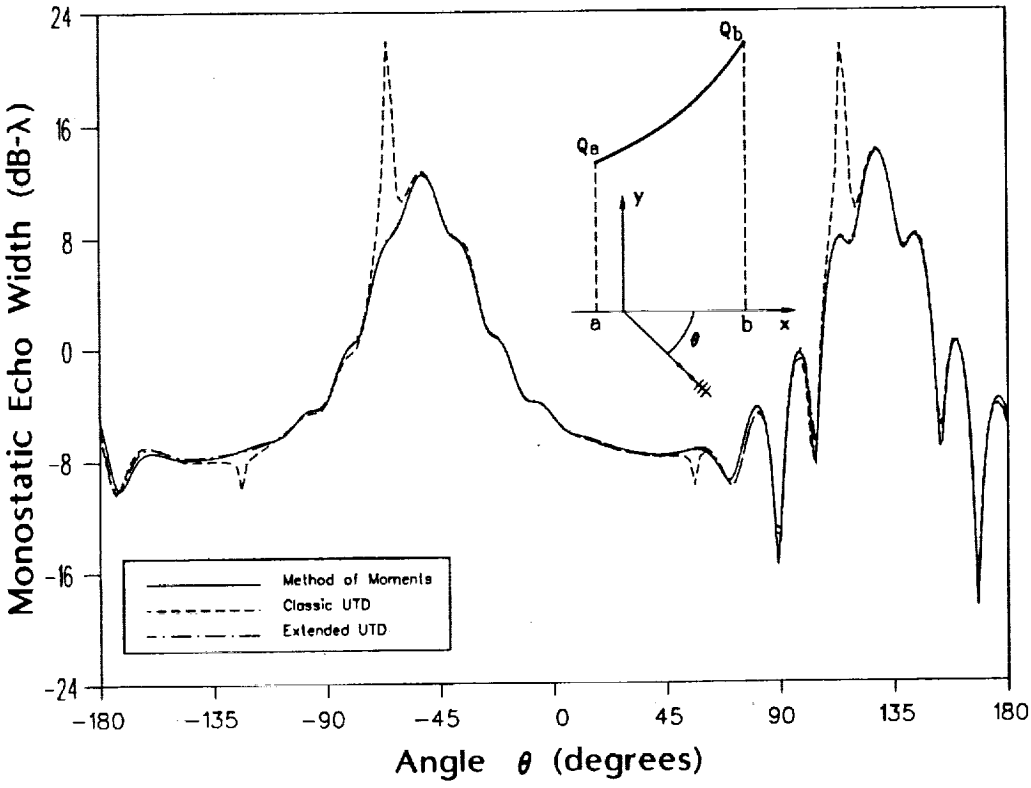

Figure 4.8: Monostatic echo width (TM polarization case) from a cubic polynomial strip with $a_0 = 2.0\lambda$, $a_1 = 0.5$, $a_2 = 0.1\lambda^{-1}$, $a_3 = 0.1\lambda^{-2}$, $a = -0.33\lambda$, and $b = 1.5\lambda$.

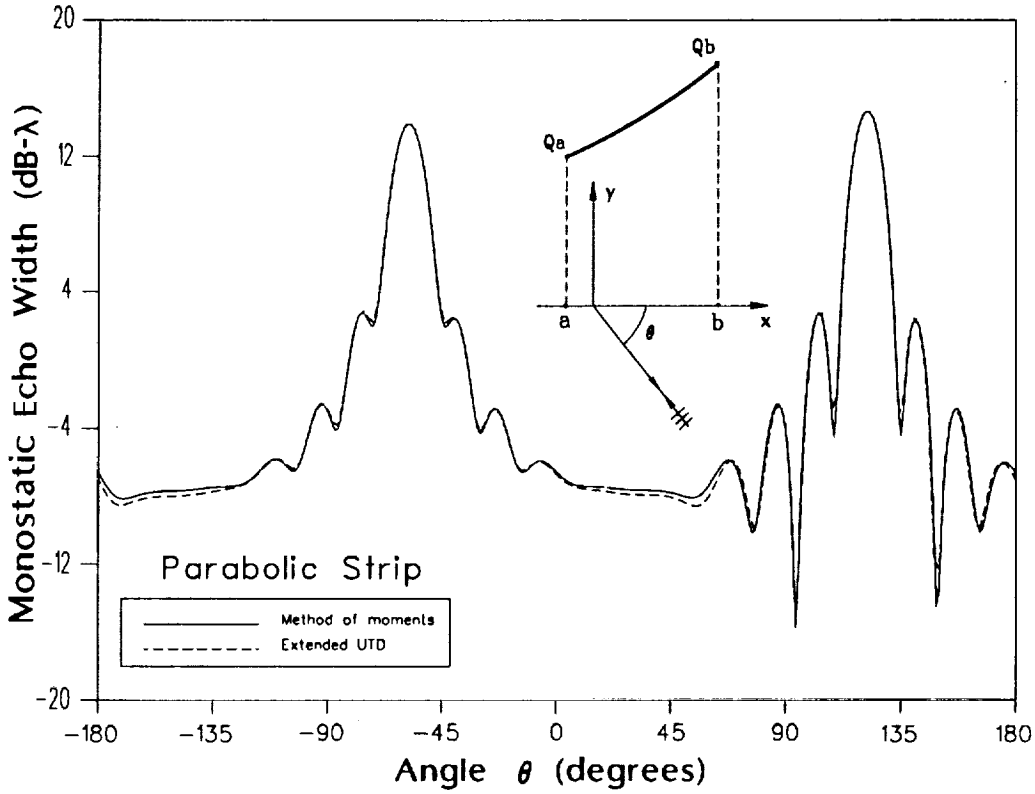

Figure 4.9: Monostatic echo width (TM polarization case) from a cubic polynomial strip with $a_0 = 2.0\lambda$, $a_1 = 0.5$, $a_2 = 0.1\lambda^{-1}$, $a_3 = 0.0\lambda^{-2}$ (parabolic strip), $a = -0.33\lambda$, and $b = 1.5\lambda$.

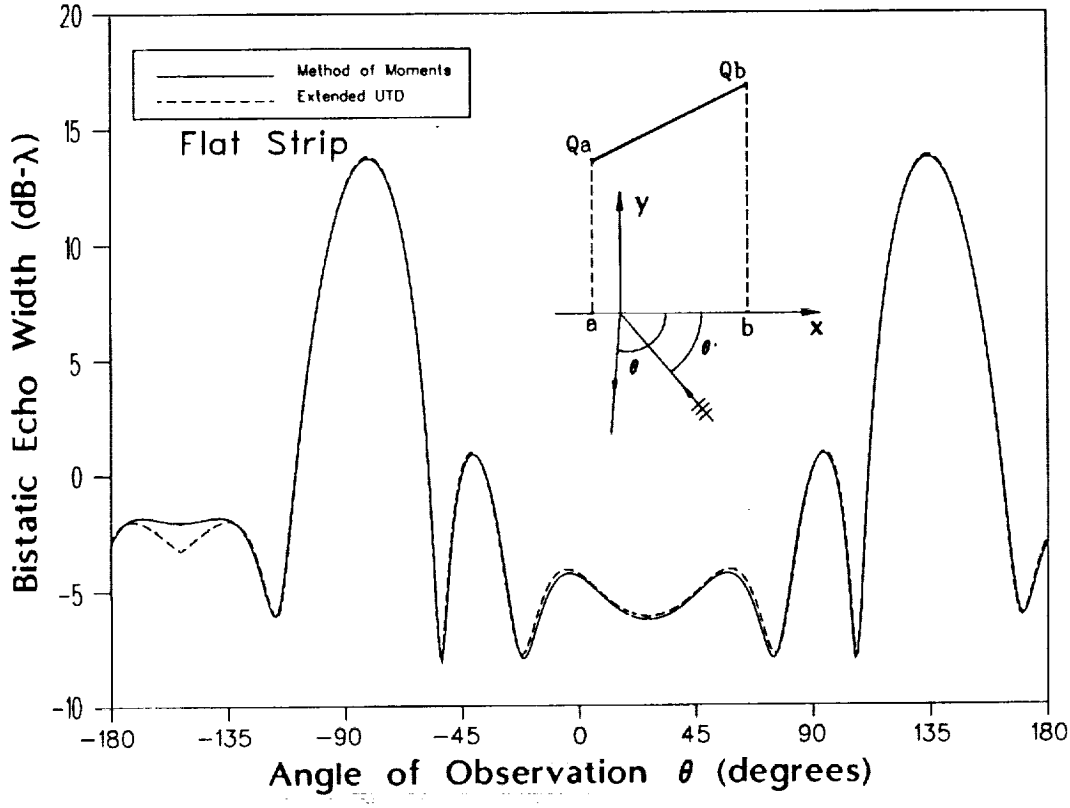

Figure 4.10: Bistatic echo width (TM polarization case) from a cubic polynomial strip with $a_0 = 2.0\lambda$, $a_1 = 0.5$, $a_2 = 0.0\lambda^{-1}$, $a_3 = 0.1\lambda^{-2}$ (flat strip), $a = -0.33\lambda$, $b = 1.5\lambda$, and angle of incidence $\theta' = -45°$.

Chapter 5

Summary and Conclusions

We have presented an extended UTD solution for the scattering and diffraction from cubic polynomial boundaries containing edges. This new solution involves the incomplete Airy integrals as canonical functions and effectively describes the transitional field behavior associated with composite shadow boundaries and caustics of the reflected rays. The total solution is presented in a ray optical format by deriving the appropriate uniform reflection, zero-curvature and edge diffraction coefficients that remain valid inside the transition regions, and also provide smooth connection into the regions where the classic ray optical formulations remain valid.

It was shown by comparison with a reference method of moments solution that the extended UTD TM polarization solution yields excellent results. The TE polarization solution also showed good agreement with the reference solution although it would benefit from the inclusion of higher order effects such as edge excited creeping waves, double edge diffraction, and whispering gallery modes in certain regions where grazing fields exist. The failure of classic UTD solution to describe the scattered fields near caustics of the reflected rays and composite shadow boundaries was also clearly illustrated. The universal nature of the extended UTD solution was demonstrated by considering examples of a parabolic screen and a flat strip. In both special cases, the new solution gave excellent results. Therefore, the extended UTD

solution can be used to effectively describe the scattered fields from general curved surfaces ranging from strictly concave or convex, concave-convex, or completely flat.

Appendix A

Ordinary Airy Functions

The ordinary Airy functions satisfy the following differential equation:

$$y''(\sigma) - \sigma y(\sigma) = 0 \tag{A.1}$$

which has two independent solutions, $\mathrm{Ai}(\sigma)$ and $\mathrm{Bi}(\sigma)$. In integral form they are given by

$$\mathrm{Ai}(\sigma) = \frac{1}{2\pi}\int_{L_{21}} e^{j(\sigma z + z^3/3)}\,dz \tag{A.2}$$

$$\mathrm{Bi}(\sigma) = \frac{j}{2\pi}\int_{L_{23}+L_{13}} e^{j(\sigma z + z^3/3)}\,dz \tag{A.3}$$

where the contours of integration L_{21}, L_{23} and L_{31} are shown in Figure A.1. For small arguments they can be computed using their ascending series form [14], i.e.,

$$\mathrm{Ai}(\sigma) = c_1 f(\sigma) - c_2 g(\sigma) \tag{A.4}$$

$$\mathrm{Bi}(\sigma) = \sqrt{3}[c_1 f(\sigma) + c_2 g(\sigma)] \tag{A.5}$$

where

$$f(\sigma) = 1 + \frac{1}{3}\sigma^3 + \frac{1\cdot 4}{6}\sigma^6 + \frac{1\cdot 4\cdot 7}{9}\sigma^9 + \cdots \tag{A.6}$$

$$g(\sigma) = \sigma + \frac{2}{4}\sigma^4 + \frac{2\cdot 5}{7}\sigma^7 + \frac{2\cdot 5\cdot 8}{10}\sigma^{10} + \cdots \tag{A.7}$$

$$c_1 = \mathrm{Ai}(0) = \mathrm{Bi}(0)/\sqrt{3} = 3^{-2/3}/\Gamma(2/3) \tag{A.8}$$

$$c_2 = \mathrm{Ai}'(0) = \mathrm{Bi}'(0)/\sqrt{3} = 3^{-1/3}/\Gamma(1/3)\,. \tag{A.9}$$

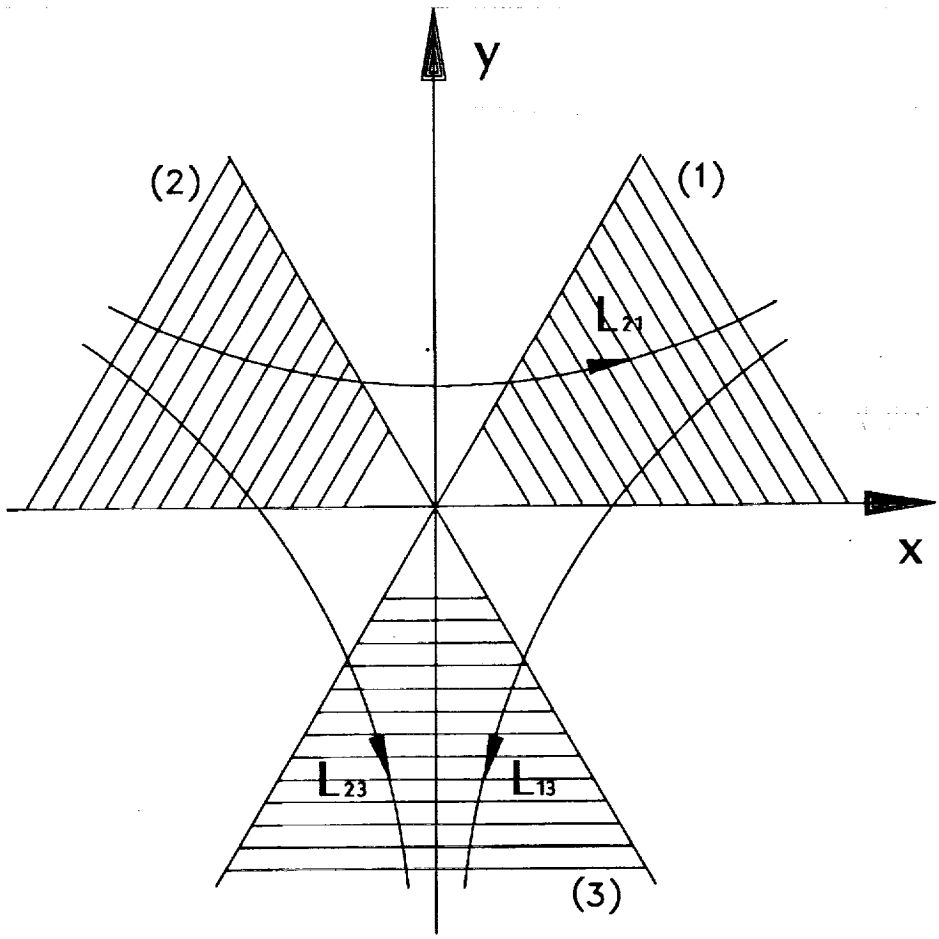

Figure A.1: Contours of integration for the ordinary Airy Functions.

Their large argument forms are given by

$$\mathrm{Ai}(\sigma) \sim \frac{1}{2}\pi^{-1/2}\sigma^{-1/4}e^{-\frac{2}{3}\sigma^{3/2}} \qquad (|\arg\sigma| < \pi) \tag{A.10}$$

$$\mathrm{Ai}(-\sigma) \sim \pi^{-1/2}\sigma^{-1/4}\sin\left(\frac{2}{3}\sigma^{3/2}+\frac{\pi}{4}\right) \qquad (|\arg\sigma| < 2\pi/3) \tag{A.11}$$

$$\mathrm{Bi}(\sigma) \sim \pi^{-1/2}\sigma^{-1/4}e^{\frac{2}{3}\sigma^{3/2}} \qquad (|\arg\sigma| < \pi/3) \tag{A.12}$$

$$\mathrm{Bi}(-\sigma) \sim \pi^{-1/2}\sigma^{-1/4}\cos\left(\frac{2}{3}\sigma^{3/2}+\frac{\pi}{4}\right) \qquad (|\arg\sigma| < 2\pi/3)\,. \tag{A.13}$$

Complete asymptotic expansions may be found in [14].

Appendix B

Incomplete Airy Functions

The incomplete Airy functions satisfy the parabolic differential equation applied by Fock [15] and others to the study of fields near the surface of convex diffracting bodies, i.e.,

$$\left[\frac{\partial^2}{\partial\sigma^2} - \sigma - j\frac{\partial}{\partial\gamma}\right] y(\sigma,\gamma) = 0 \tag{B.1}$$

which has three independent solutions, $g_i(\sigma,\gamma)$, $i = 1,2,3$. In integral form they are given by

$$g_i(\sigma,\gamma) = \int_{\gamma}^{\infty \exp(j\psi_i)} e^{j(\sigma z + z^3/3)}\, dz \;; \quad i = 1,2,3 \tag{B.2}$$

where the contours of integration are shown in Figure B.1. The functions g_2 and g_3 can be obtained from g_1 and the ordinary Airy functions as follows:

$$g_2(\sigma,\gamma) = g_1(\sigma,\gamma) - 2\pi \mathrm{Ai}(\sigma), \quad \text{and} \tag{B.3}$$

$$g_3(\sigma,\gamma) = g_1(\sigma,\gamma) - \pi[\mathrm{Ai}(\sigma) + j\mathrm{Bi}(\sigma)]. \tag{B.4}$$

For small values of σ, g_1 can be computed using its ascending series form [9], i.e.,

$$g_1(\sigma,\gamma) = \sum_{n=0}^{\infty} a_n(\gamma)\sigma^n \tag{B.5}$$

where

$$a_0(\gamma) = g_1(0,\gamma) = e^{j\pi/6} 3^{-2/3} \Gamma(1/3, -j\gamma^3/3), \tag{B.6}$$

$$a_1(\gamma) = \frac{\partial}{\partial\sigma} g_1(0,\gamma) = -e^{-j\pi/6} 3^{-1/3} \Gamma(2/3, -j\gamma^3/3), \tag{B.7}$$

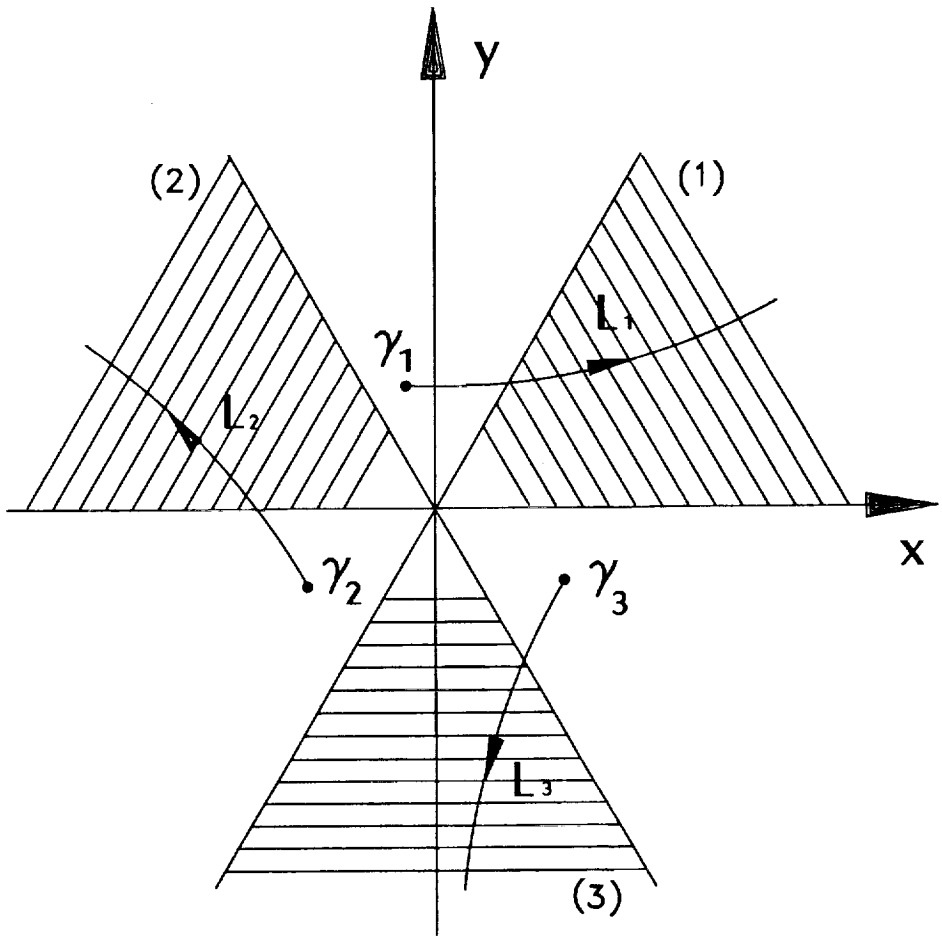

Figure B.1: Contours of integration for the incomplete Airy Functions.

$$a_2(\gamma) = \frac{j}{2}a_0'(\gamma), \tag{B.8}$$

$$a_n(\gamma) = \frac{a_{n-3}(\gamma) + ja_{n-2}'(\gamma)}{n(n-1)}, \quad n \geq 3 \tag{B.9}$$

and $\Gamma(x,y)$ is the incomplete Gamma function. The asymptotic forms of g_1 are given by

$$g_1(\sigma,\gamma) \sim \frac{j}{\sigma+\gamma^2}e^{j(\sigma\gamma+\gamma^3/3)} \qquad (\gamma \gg |\sigma|^{1/2}) \tag{B.10}$$

$$g_1(\sigma,\gamma) \sim \frac{e^{-j\frac{2}{3}(-\sigma)^{3/2}}}{(-\sigma)^{1/4}}\left[\sqrt{\pi}e^{j\frac{\pi}{4}}u(-\eta) - \frac{F^*(\eta^2)}{2j\eta}e^{j\eta^2}\right] - \frac{1}{2j}\left[\frac{2}{\sigma+\gamma^2} - \frac{1}{\eta(-\sigma)^{1/4}}\right]e^{j(\sigma\gamma+\gamma^3/3)} \qquad (\sigma \ll -1) \tag{B.11}$$

where

$$\eta = \pm\left[\sigma\gamma + \gamma^3/3 + \frac{2}{3}(-\sigma)^{3/2}\right]^{1/2}; \quad \gamma_<^>(-\sigma)^{1/2} \tag{B.12}$$

and $F(x)$ is the Kouyoumjian-Pathak transition function [5]. Complete asymptotic expansions for g_1 along with some representative plots may be found in [9].

Bibliography

[1] Crispin, J. W., and Siegel, K. M., *Methods of Radar Cross-Section Analysis,* New York, Academic Press, 1968.

[2] Harrington, R. F., *Field Computation by Moment Methods,* Robert E. Krieger Publishing Company, 1968.

[3] Kline, M., and Kay, I. W., *Electromagnetic Theory and Geometrical Optics,* Interscience Publishers, Inc., 1965.

[4] Keller, J. B., "Geometrical Theory of Diffraction," *J. Opt. Soc. of America,* Vol. 52, No. 2, pp. 116-130, Feb. 1962.

[5] Kouyoumjian, R. G. and Pathak, P. H. "A Uniform Geometrical Theory of Diffraction for an Edge in a Perfectly Conducting Surface," *Proc. of IEEE,* Vol. 62, pp. 1448-1461, Nov. 1974.

[6] Levey, L. and Felsen, L. B., "On Incomplete Airy Functions and their Application to Diffraction Problems," *Radio Science,* Vol. 4, No. 10, pp. 959-969, Oct. 1969.

[7] Pathak, P. H. and Liang, M. C., "On a Uniform Asymptotic Solution Valid Across Smooth Caustics of Rays Reflected by Smoothly Indented Boundaries," *IEEE Trans. Antennas Propagat.,* Vol. 38, No. 8, pp. 1192-1203, Aug. 1990.

[8] James, G. L., *Geometrical Theory of Diffraction for Electromagnetic Waves,* p. 37, Peter Peregrinus Ltd., London, UK, 1976.

[9] Constantinides, E. D. and Marhefka, R. J., "Efficient and Accurate Computation of the Incomplete Airy Functions," to appear in *Radio Science.*

[10] Chester, C., Friedman, B. and Ursell, F., "An Extension of the Method of Steepest Descent," *Proc. Cambridge Phil. Soc.,* Vol. 53, pp. 599-611, 1957.

[11] Ikuno, H. and Felsen, L. B., "Real and Complex Rays for Scattering from a Target with Inflection Points," *Radio Science,* Vol. 22, No. 6, pp. 952-958, Nov. 1987.

[12] Ikuno, H. and Felsen, L. B., "Complex Ray Interpretation of Reflection from Concave-Convex Surfaces," *IEEE Trans. Antennas Propagat.,* Vol. 36, pp. 1260-1271, Sept. 1988.

[13] James, G. L., *Geometrical Theory of Diffraction for Electromagnetic Waves,* p. 150, Peter Peregrinus Ltd., London, UK, 1976.

[14] Abramowitz, M. and Stegun, I. A., editors, *Handbook of Mathematical Functions,* Dover Publications, Inc., pp. 446-452, New York, 1972.

[15] Fock, V. A., *Electromagnetic Diffraction and Propagation Problems,* Pergamon, Oxford, England, 1965.

725311-2, " An Extended UTD Analysis for the Scattering and Diffraction from Cubic Polynomial Strips", Constantinides and Marhefka, 1/93